

Neuro-evolutionary evidence for a universal fractal primate brain shape

Yujiang Wang^{1,2,3*}, Karoline Leiberg¹, Nathan Kindred ², Christopher R. Madan⁴,
Colline Poirier², Christopher I. Petkov^{2,5}, Peter N. Taylor^{1,2,3*}, Bruno C.C. Mota⁶

September 19, 2022

1. CNNP Lab (www.cnnp-lab.com), Interdisciplinary Computing and Complex BioSystems Group, School of Computing, Newcastle University, Newcastle upon Tyne, United Kingdom
2. Faculty of Medical Sciences, Newcastle University, Newcastle upon Tyne, United Kingdom
3. UCL Institute of Neurology, Queen Square, London, United Kingdom
4. Department of Neurosurgery, University of Iowa
5. School of Psychology, University of Nottingham, Nottingham, United Kingdom
6. metaBIO Lab, Instituto de Física, Universidade Federal do Rio de Janeiro (UFRJ), Rio de Janeiro, Brazil

* Yujiang.Wang@newcastle.ac.uk

Abstract

The primate cerebral cortex can take on a bewildering diversity of shapes and sizes within and across species, whilst maintaining archetypal qualities that make it instantly recognisable as a “brain”. Here we present a new way of expressing the shape of a cortex explicitly as the hierarchical composition of structures across spatial scales. In computational simulations, as one successively removes sulci and gyri smaller than a specified scale, the cortices of 11 primate species are gradually coarse-grained into less folded brains until lissencephaly (no folding). We show that this process, in all cases, occurs along a common scale-free morphometric trajectory overlapping with other mammalian species, indicating that these cortices are not only approximately fractal in shape, but also, strikingly, are approximations of the *same* archetypal fractal shape. These results imply the existence of a single universal gyrification mechanism that operates in a scale-free manner on cortical folds of all sizes, and that there are surprisingly few effective degrees of freedom through which cortical shapes can be selected for by evolution. Finally, we demonstrate that this new understanding can be of practical use: biological processes can now be interrogated in a highly scale-dependent way for increased sensitivity and precision. To our knowledge, this is the most parsimonious universal description of the brain’s shape that is at the same time mechanistically insightful, practically useful, and in full agreement with empirical data across species and individuals.

1 Introduction

The morphological complexity of the mammalian cerebral cortex has puzzled scientists for generations, with cortices across and within species exhibiting a large diversity of shapes and sizes. Such diversity is not arbitrary, however. The mammalian brain folds into stereotypical, hierarchically-organized structures such as lobes and major gyri. In fact, qualitative and quantitative regularities in cortical scaling have often been suggested and observed (Francis et al., 2009; Karbowski, 2011; Mota and Herculano-Houzel, 2014; Zhang and Sejnowski, 2000). More specifically, through modelling the mechanism of cortical folding from a statistical physics approach, we have derived a theoretical scaling law relating pial surface area A_t , exposed surface area A_e , and average cortical thickness T :

$$A_t T^{\frac{1}{2}} = k A_e^{\frac{5}{4}}. \quad (1)$$

This relationship was shown to be valid across mammalian species (Mota and Herculano-Houzel, 2015) and within the human species (Wang et al., 2016), as well as to the structures and substructures of individual brains (Wang et al., 2019). Notably, across all these cases the dimensionless offset k is shown to be near invariant. However, this universality, presumed to be arising from universal physical principles and evolutionarily conserved biomechanics, says little about what that cortical shape actually is, beyond a constraint binding three morphometric parameters.

In this paper, we take Eqn. (1) as an empirical starting point, regardless of the hypothesised gyrification mechanism¹, to create a new, elegant and hierarchical way of expressing cortical shape. Specifically, we introduce a surface integrity-preserving coarse-graining procedure that will render cortical shapes at different spatial scales, or resolutions. We show that the *shape of primates (and possibly all mammal) cerebral cortices at each spatial scales can be understood as approximations of the same universal self-similar archetypal form*, of which the observed scaling law (Eqn. 1) can then be shown to be a direct consequence.

Besides revealing a symmetry in nature hidden under much apparent complexity, the universality indicates a very limited number of variables for evolution to tune, which in turn allows for

¹Many alternatives of which have been proposed (see (Essen, 1997; Quezada et al., 2020; Tallinen et al., 2014), reviewed in (Llinares-Benadero and Borrell, 2019; Ronan and Fletcher, 2014)), albeit without so far replicating the empirically confirmed scaling in Eqn. (1)

a principled scientific approach to analysing brain shape across evolution. These results further provide us with a new and powerful tool to express and analyze cortical morphology, even on an individual basis. As an example, we will use it later to calculate the effects of human aging across spatial scales and show that the effects are extremely scale-dependent.

2 Methods

The universal scaling law (Eqn. 1) can be rewritten in a suggestive way

$$\frac{A_t}{A_0} = \left(\frac{A_e}{A_0} \right)^{1.25}, \quad (2)$$

where the $A_0 = \frac{T^2}{k^4}$ is a fundamental area element that defines the threshold between gyrencephaly and lissencephaly, and $A_t = A_e = A_0$. For a constant k the value of A_0 is a multiple of T^2 , indicating that cortical thickness determines the size of the smallest possible gyri and sulci.

This re-writing suggests a new perspective, or interpretation of the scaling law: it now suggests a relationship between intrinsic and extrinsic measures of cortical size²: A_t and A_e respectively, measured in units of A_0 . This is reminiscent of fractal scaling (Mandelbrot, 1983), where a complex shape reveals ever smaller levels of self-similar detail as it is probed in ever smaller scales (or equivalently, higher resolutions), represented here by A_0 . The scaling exponent between the measured intrinsic and extrinsic sizes is the so-called fractal dimension.

Although actual fractals are mathematical abstractions, they can often be defined as the limit of iterative processes. Many structures in nature, and in particular biology (Di Ieva, 2016; Elston and Zietsch, 2005; Ionescu et al., 2009; Klonowski, 2016; Losa, 2011; Plank and Benhamou, 2008; Reznikov et al., 2018), are good approximations of some iterate of a fractal. Equation (2) is suggestive, but not proof, that cortices are among these forms, with a fractal dimension of $1.25 \times 2 = 2.5$ (the factor 2 is the topological dimension of areas). Indeed, fractal scaling for various aspects of cortical morphology has been often postulated (Free et al., 1996; Kiselev et al., 2003), with a number of recent papers making use of MRI data (Jao et al., 2021; Marzi et al., 2021). Most

²Given the folded laminar structure of the cortex, areas are the more natural way of measuring its size

recently published estimates of fractal dimension for the whole cortex are indeed close to 2.5 (Madan and Kensinger, 2016; Marzi et al., 2020).

Here, for the first time, we show how to directly construct morphologically plausible realisations of cortices at any specified spatial scale, or resolution. We achieve this with a coarse-graining procedure that removes morphological details smaller than a specified scale while preserving surface integrity. For example, at a set scale of 3mm, sulcal walls that are less than 3mm apart would be removed, and the neighbouring gyri could be fused. This method is a new systematic way of expressing cortical shape, in terms of a flow of morphometric measurements as spatial scale vary. By examining how areas scale across coarse-grained realisations of actual primate cortices, we will be able to directly verify cortical self-similarity.

Our method requires the bounding pial and white matter surfaces of the cortical ribbon as input. We obtained these surfaces based on reconstructions from magnetic resonance imaging data in 11 different primate species (see Suppl. S1). Algorithmically, we then segment the space between the original pial and white matter surfaces into a 3D grid of cubes of the desired scale λ , where each cube is of dimensions $\lambda \times \lambda \times \lambda$. We also term the 3D grid of cubes “voxelisation”, as it effectively captures the shape of the cerebral cortex as voxels in 3D space. At any given scale, or voxel size, this process effectively erases morphological features (folds) that are smaller than the cube size. Visually, increasing the voxel size appears as if the cortex is “melting” (Fig. 1).

In detail, we assign all voxels in the grid with at least four corners inside the original pial surface to the pial voxelization. We then assign voxels with all eight corners inside the original white matter surface to the white matter voxelization. Finally, subtracting the white matter voxelisation from the pial voxelisation, we obtain the grey matter voxelisation (Fig. 1B bottom row). The pial surface voxelisation is designed such that neighbouring gyri can fuse if their separation is smaller than the scale of interest, whilst not growing the cortex outwards. The white matter surface voxelisation allows the walls of each gyrus to thicken and fuse inwards. Visually, iterating this process looks as if the cortex is “thickening” inwards and smoothing on the outside.

From the voxelised cortex at each scale λ , we can then obtain coarse-grained pial and white matter surfaces, and extract estimates of global morphometric measures such as the average cortical

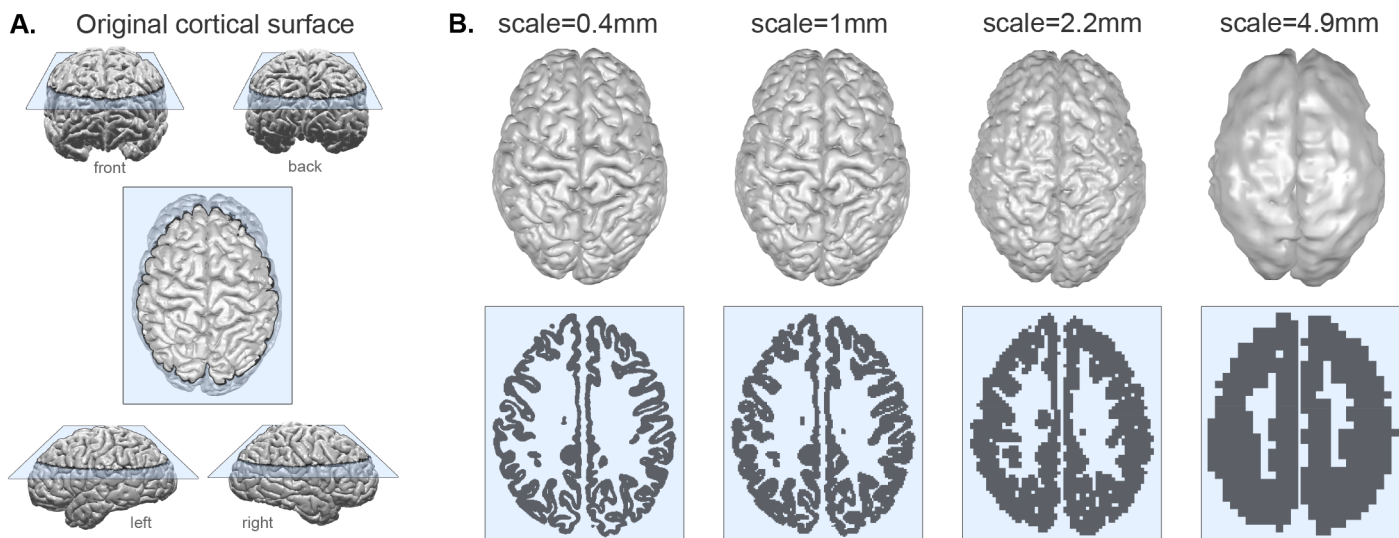


Figure 1: Coarse-graining a cortex at different scales. **A:** Example original pial surface from a healthy human viewed from angles. **B:** Same example cortical surface from A, coarse-grained to different spatial scales. Top row shows resulting pial surfaces (with a small amount of smoothing applied for visualisation purposes here). Bottom row shows the corresponding voxelisation at each scale through the slice indicated by blue plane in panel A.

thickness $T(\lambda)$, the total cortical surface area $A_t(\lambda)$, and the exposed surface area $A_e(\lambda)$. For each λ , we derived an outer isosurface equal to 0.5 for the pial voxelisation (voxel values are 1 within the voxelised pial surface and 0 otherwise). This isosurface is then defined as the coarse-grained pial surface at this scale. The surface area of this isosurface is used as $A_t(\lambda)$. The exposed surface area $A_e(\lambda)$ is subsequently derived from the convex hull of the pial isosurface. Finally, the cortical thickness $T(\lambda)$ is estimated as $\frac{V_G(\lambda)}{A_t(\lambda)}$, where $V_G(\lambda)$ is the estimated grey matter volume, derived from the number of grey matter voxels times the voxel volume. These global morphometric measures are summary statistics of the shape of the brain at each particular scale, capturing information about both their intrinsic geometry ($A_t(\lambda), T(\lambda)$) and extrinsic geometry ($A_e(\lambda)$). In this manner, for each cortex, we obtain not just one set of summary morphometric measures, but rather an successive set measures as functions of λ . A detailed walk-through of the coarse-graining algorithm and estimation of morphometric measures is provided on Github: <https://github.com/cnp-lab/CorticalFoldingAnalysisTools/blob/master/Scales/>.

Note that this process is substantially different from existing approaches measuring the fractal dimension of cortex. We do not simply apply successive convolution with an increasing kernel size (or equivalent), which effectively would achieve a uniform and spatially isometric “smearing” of the

original cortical shape to a given scale, rather than a targeted erasure of *surface* details smaller than said scale. As a result, this method yields well-defined and well-behaved white and gray matter surfaces. Thus, one can apply all the usual analytical tools to these realisations that are applicable to actual cortices. Note that our approach is more comparable in its principles to the calculation of the outer smoothed pial surface in Freesurfer (Schaer et al., 2008). Of course, our proposed procedure is not the only conceivable way to erase shape details below a given scale. However, it requires no fine-tuning, is computationally feasible and conceptually simple, thus making it a natural choice. We will discuss alternatives and possible extensions in Section 4.

Finally, to analyse the scaling behaviour of the different coarse-grained realisations of the same brain, we apply an isometric rescaling process that leaves all dimensionless shape properties unaffected (more details in Suppl. S2.1). Conceptually, this process fixes the voxel size, by resizing $A_t(\lambda)$, $A_e(\lambda)$ and $T^2(\lambda)$ by a factor proportional to λ^2 . This step ensures that we can compare the coarse-grained realisations to the original cortices, and test if the former, like the latter, also scale as in Eqn. (1).

3 Results

3.1 All primate brains obey the same scaling law across spatial scales

We have analysed cortices of 11 different primate species (see Suppl. S1): aotus, cebus, chimpanzee, colobus, galago, human, lagotrix, lophocebus, macaque, marmoset, and pithecia, and various cohorts of human subjects. We applied our coarse-graining procedure to their pial and white matter surfaces, and empirically determined (i) that all species followed a power law (linear regression $R^2 > 0.999$ for all species); (ii) the slope of said power law is $\alpha = 1.255$ on a group level (CI: [1.254 1.256]) using linear mixed effect modelling (see Fig. 2 for visualisation, and Suppl. S2 for a detailed breakdown by species); and importantly, (iii) all species also show a similar offset $\log k \approx -0.65263$, with a standard deviation of intercept across species estimated at 0.02 from linear mixed effect modelling.

Taken separately, the scaling for each species is proof that their cortices are self-similar with

the same scaling: they each approximate a fractal with fractal dimension $d_f = 2.5$. Taken all species together, given the near invariance of the offset k and the ensuing near overlap of the plots in Fig. 2, this is proof that all the original cortices and their coarse-grained realisations are approximations of the *same* archetypal fractal form. Thus, as Fig. 2 vividly illustrates, the data supports a *universal* scaling law across primate species and spatial scales:

$$A_t(\lambda)T(\lambda)^{\frac{1}{2}} = kA_e(\lambda)^{\frac{5}{4}}, \quad (3)$$

with $k = 0.2277$.

As a way of negative control, we also applied our voxelisation procedure to a walnut shape (see Suppl. S3). While the shape of the brain has been likened to a walnut before, we observe a distinctly lower slopes (walnut 1: $\alpha = 1.191$, $CI = [1.185 \ 1.196]$; walnut 2: $\alpha = 1.193$, $CI = [1.187 \ 1.198]$) than the primate brains, and a varying offset. This result demonstrates that the scaling 3 is indeed a characteristic of the primate brains we studied, and is not an artifact of the voxelisation procedure.

Given the demonstrated overlap between species, and if their cortices are all approximations of the same form, how can one tell apart their cortices? The answer is that all approximations have a range of validity, which varies between cortices. For a gyrified cortex of area A_t ³, the coarse-graining will remove details of ever-increasing scale, lowering $A_t(\lambda)$ until attaining lissencephaly for $A_e(\lambda_{lys}) = A_t(\lambda_{lys})$. Indeed, it follows from rewriting Eqn. (3) in the form of Eqn. (2) that a given cortex' shape will be comprised of self-similar structures with areas ranging from $A_0 = g^{-5}A_t$ at their smallest to A_t at their largest, where g is the gyrification index $g = \frac{A_t}{A_e}$. Whenever this self-similar scaling is valid, A_0 acquires a further interpretation as the typical size of the smallest structures in a cortex: patches smaller than that must be approximately smooth. Consequently, $N_{structures} \simeq \frac{A_t}{A_0} = g^5$ estimates the number of morphological features in each cortex (and adds a new interpretation for the gyrification index). For example, we estimate the human in our dataset to have about 105 morphological features in each cortical hemisphere, and the galago to have about 4 such morphological features. The corresponding $N_{structures}(\lambda)$ estimates how this number

³When no dependence on λ is indicated then we are referring to the values for the original cortex

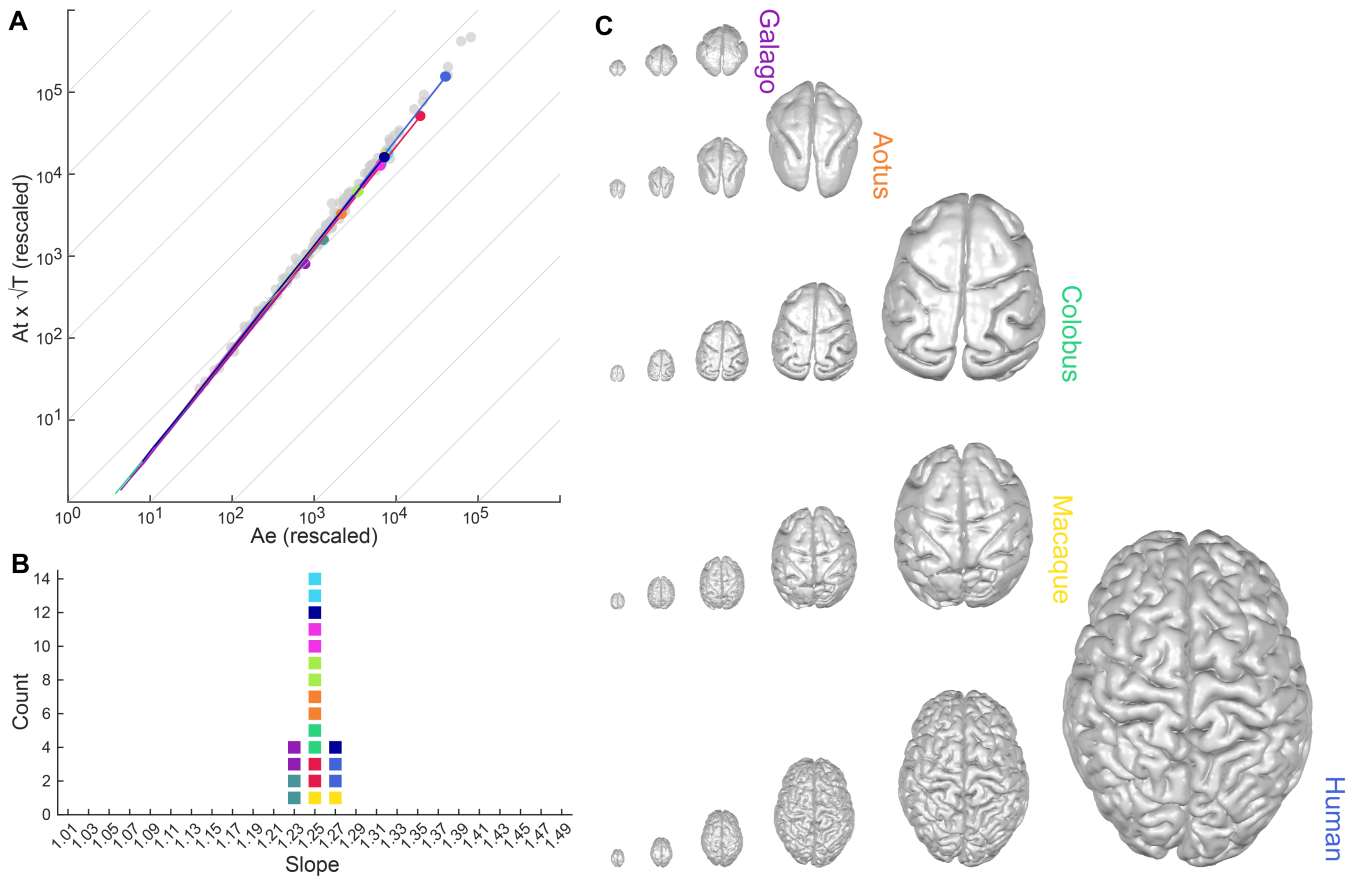


Figure 2: Scaling law of coarse-grained primate brains. **A:** coarse-grained primate brains are shown in terms of their relationship between $\log_{10}(A_t \times \sqrt{T})$ vs. $\log_{10}(A_e)$. Each solid line indicates a cortical hemisphere from a primate species. Thin grey lines indicate a slope of 1 for reference. Note that all values of A_t , A_e and T are re-scaled isometrically. Otherwise all datapoints for each species would collapse onto a vertical line of near constant A_e , see Suppl. S2 for details. Filled circles mark the data points of the original cortical surfaces in each species. Gray datapoints are plotted for reference and show the comparative neuroanatomy dataset across a range of mammalian brains (Mota and Herculano-Houzel, 2015). **B:** Slopes (α) of the regression of datapoints in A for each species shown as a dotplot. Each colour indicates a different primate species. **C:** Rescaled brain surfaces for five example species (from top to bottom: galago, aotus, colobus, macaque, and human) at different levels of coarse-graining chosen at the same level of rescaled A_e (from left to right columns indicate rescaled $\log A_e$ values of: 1.5, 2, 2.5, 3, 3.5, 4, where applicable).

changes over coarse-graining. Suppl. S6 provides a more detailed discussion on this topic.

3.2 Primate brains at different spatial scales are morphometrically similar to each other and other mammalian species

The previous section demonstrated that primate cortices are characterized by an invariant k ; by self-similar structures with a size range specified by the total area A_t , a proxy for cortical size (Mota

et al., 2019); and by the gyrification index g , a dimensionless measure of morphological complexity (Lebed et al., 2013; Rabiei et al., 2017). These variables, k , A_t and g are not independent of one another, however. Thus, in this section we will use a previously introduced (Wang et al., 2021) set of independent morphometric measures, K, I and S , that better summarize the shape of the cortex in a natural and statistically robust way. In this framework, any cortex corresponds to a point in a so-called KIS space. Isometrically scaled copies of the same shape all map onto a line along the $I = \log A_t + \log A_e + \log T^2$ direction, which is perpendicular to a $K \times S$ plane that fully summarizes their shape. $K = \log A_t - \frac{5}{4} \log A_e + \frac{1}{4} \log T^2$ is the direction defined by the offset k of the scaling law Eqn. (1). Finally, the $S = \frac{3}{2} \log A_t + \frac{3}{4} \log A_e - \frac{9}{4} \log T^2$ direction captures the remaining information about shape and can be regarded as a simple measure of morphological complexity. See (Wang et al., 2021) for detailed derivation and demonstration of the superior sensitivity and specificity of these new morphometric variables.

The I component captures all information about cortical size, and is simply an isometric scaling coefficient. Its value is thus dictated by the rescaling process (Suppl. S2.1). Therefore, in the following, we focus on its perpendicular plane, the $K \times S$ plane. When applied to different species and projected to the $K \times S$ plane (Fig. 3), the coarse-graining procedure generates trajectories that largely overlap. While S decreases with increasing scale λ , K remains nearly constant for all primate brains (note this is not true for the walnut, c.p. Suppl. S3). This is in line with our previous observation that the offset in the scaling law is extremely similar between species. In this framework, our main result can be also expressed simply: For all cortices we analyzed, and for none of the non-cortices, our coarse-graining process will leave K largely unaffected, while the morphological complexity S will decrease with coarse-graining scale. Thus, iteratively coarse-grained cortical shapes are morphometrically similar to (and in terms of the universal law ‘as valid as’) actually existing cortices. In broad terms, a human cortex, melted to a suitable scale, will resemble a Chimpanzee cortex in shape (in terms of its summary morphometric measures, if not in the details of every sulcus and gyrus); both cortices, melted some more will resemble that of a Macaque, then an Aotus, then a Galago, all the way down to a common lysencephalic cortex, corresponding to the common hemispheric external shape of cortical hemisphere (Mota et al.,

2019). At this point S will attain a universal lower value of $S_0 = k^{-9}$ (as can be derived from 3 by setting $A_t = A_e = A_0$, at the lissencephalic limit, also see Suppl. S6). All cortices analyzed are realisations of the same archetype, differing only in their scale (Mandelbrot, 1967).

In Fig. 3, we also projected the morphometric data for a comparative neuroanatomy dataset from a range of mammalian species. Again, we can see a good agreement between the coarse-grained primate cortices and a broader sample of mammalian cortices. This overlap further suggests that the archetypal shape is a general property of mammalian cortices, rather than limited to primates.

Visually and qualitatively, appropriately-scaled primate cortices with the same value of S indeed look very similar to each another, as can be seen in the example pial surfaces at the top of Fig. 3. At $S=2.2$, all brains regardless of (isometric) size are almost lissencephalic. With increasing S , all cortices become proportionally thinner and more gyrified, and the sulci become proportionally deeper. We therefore demonstrated interrelated algorithmic, geometric and biological interpretations of S : It is, respectively, a coarse-graining parameter, a measure of the overall morphological complexity of the cortical surface, and the most significant degree of freedom through which evolution can specify cortical morphology.

3.3 Morphometric measures as a function of scale reveal scale-specific effects of ageing

In the final part of our work, we show how our coarse-graining algorithm and the associated new understanding of brain morphology may become useful in applications. To this end, as an example, we will focus on how the ageing process affects human cortical morphology across scales. In Fig. 4 A, we compare $K(\lambda)$ as a function of scale λ for a young (20 year old) *vs.* an old (80 year old) group of human brains. Strikingly, the difference in K between the groups take a U shape, where the strongest positive effect is seen at sub-millimeter scales (0.2mm; younger subjects indeed have a higher K , as previously shown in (Wang et al., 2016)), but the effect reverses itself and turns negative at millimeter scales (older subjects have higher K), peaking at about 2mm. For scales over 5mm the differences become negligible, suggesting the aging process has little

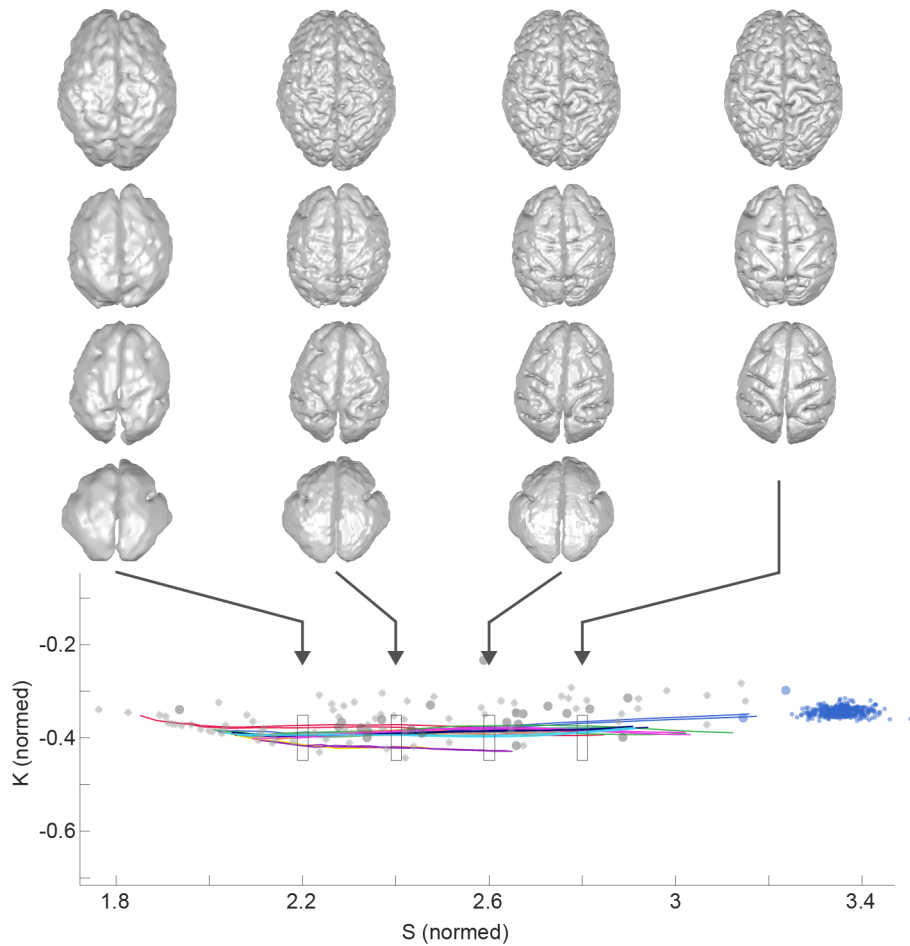


Figure 3: Morphometric similarity of coarse-grained primate cortices, other mammalian and human brains in $K \times S$ plane. Top: Human, macaque, cebus, and galago brains (from top row to bottom row) coarse-grained at different scales with corresponding different values of S . **Bottom:** $K \times S$ plane showing the coarse-grained primate brains (same as in Fig. 2) as solid lines, and different mammalian brains from comparative neuroanatomy measurements ((Mota and Herculano-Houzel, 2015)) as grey disks. The larger disks indicate primate species, the smaller disks other mammalian (non-primate) species. Adult human datapoint are shown as blue disks. HCP datapoints derive from T1w imaging (see (Wang et al., 2019)) are shown as smaller blue disks. Note the $K \times S$ plane is shown with normalised K and S , which ensured that magnitudes in K and S are directly comparable. The variation in S is much larger than in K for primate coarse-grained brains.

effect on the larger cortical morphological features. This result demonstrates clearly that different types of morphometric information are revealed at certain scales but not in others. Therefore, to understand the ageing process in terms of cortical morphology, analysing cortical morphometric measures across spatial scales may be not just informative, but *crucial*. This also implies that there may be an optimal scale to detect certain biological effects, and that one may combine information across multiple scales in ways that are optimized to differentiate groups across development, age or disease.

In this particular example, the dramatic change in the effect of K can be visually and intuitively understood by looking at changes in total surface area (Fig. 4 B, also see Suppl. S4): Fig. 4 C shows some cross-sectional images of the cortical surface, and we see that at scale 0.27 mm, the gyri in the younger subjects are densely packed, but the older subjects show the expected (see e.g. (Jin et al., 2018; Madan, 2019) for recent investigations and references therein) widening between gyral walls and decrease in gyral surface area at the crown. Hence the younger subjects show an increased overall surface area. At 1.86mm, the younger cortices have already partially “melted”, erasing most small sulci between the densely packed gyri. In the older humans, however, the gyri are less dense, the sulci more open, and thus, at 1.86mm, most gyri and sulci have not been erased yet. Hence, coarse-graining strongly decreases surface area in the younger humans compared to the older humans at this scale. At scale 7.94mm, both young and old brains have “melted” down to very similar near-lissencephalic shapes, and indeed show a similar total surface area.

More broadly, one can regard the melting process as a way of determining how cortical area is allocated across different scales. As the cortex ‘melts’, the contributions to the total area from features smaller than the cut-off scale are eliminated. In the example in Fig. 4, for instance, we can say about half ($10^{5-4.7} = 10^{0.3} \approx 2$) the total area in the 80 y.o. cortices is present in features smaller than 4mm.

These results on ageing are also reproduced in an independent dataset in Suppl. S5.

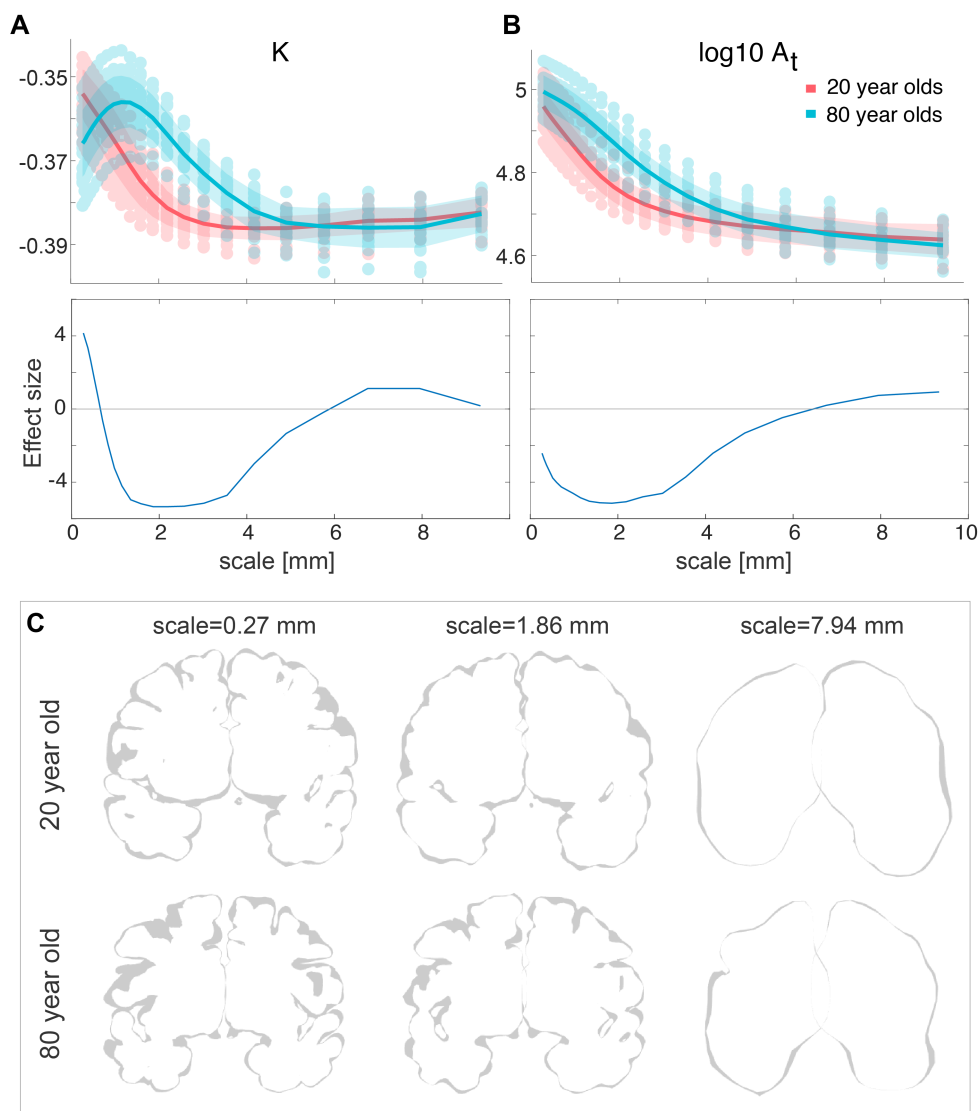


Figure 4: Human ageing shows differential effects depending on spatial scale. **A:** Top: $K(\lambda)$ is shown for a group of 20 year olds (red) and a group of 80 year olds (blue). Individual data points show individual subjects. Mean and standard deviation are shown as the solid line and the shaded area respectively. Bottom: Effect size (measured as ranksum z-values) between the older and younger groups at each scale. Positive effect indicates a larger value for the younger group. **B:** Same as A, but for $\log_{10} A_t$ (without rescaling). **C:** Coronal slices of the pial surface of a 20 year old and a 80 year old at different scales (columns).

4 Discussion

We have devised a new way of expressing the shape of the mammalian cerebral cortex, as the flow in the values of a triad of morphometric measures when each cortex is rendered over a range of spatial scales. This was achieved by successively coarse-graining the cortex, erasing morphological features smaller than the specified scale, while preserving cortical surface integrity. After applying

this method to the cortices of 11 primate species, we have shown that all these diverse shapes are specific approximation of *same archetypal self-similar (fractal) shape*; and, conversely, most of their morphological diversity can be ascribed to the different ranges of spatial scales over which said approximation is valid in each case.

This new morphological syntax, the algorithm used to generate it, and the empirical result thus obtained, have significant implications, to which we now turn.

Expressed in this syntax, a folded structure can be informally described by its size (isometric size $I(\lambda)$) and shape (morphological complexity $S(\lambda)$ and offset $K(\lambda)$) when rendered at varying resolutions (spatial scale λ). Cortices, in particular, are characterized by a near-constant value $K(\lambda) \cong K$ across species. This way of expressing morphology is more detailed than a list of summary morphometric measures, and more informative than the mere listing of every sulci and gyri. We suggest that this syntax as suggested here, may form the basis of a more holistic approach of characterising brain morphology and morphological changes. A clear advantage is the different biological processes may only act on a specific spatial scale, whilst leaving other scales largely untouched (ageing in our example). By disambiguation of the spatial scale, it allows for an extra dimension of understanding, and tracking of biological processes (e.g. healthy ageing vs. dementia may play out on different spatial scales, allowing for scale-specific biomarkers). In the future, this approach can also be extended also to cortical development and to various degenerative (Wang et al., 2016) and congenital (Wang et al., 2021) neuropathic conditions, especially if combined with a regionalized version of this method applied to specific cortical regions (Wang et al., 2019) or local patches (Leiberg et al., 2021).

The coarse-graining algorithm provides us with a sequence of realisations of each cortex, ranging from the original image to its eventual lissencephalic limit. By ensuring the integrity and preventing self- and mutual-intersecting of its limiting surfaces, we are able to apply all the tools and methods applicable to actual cortices also to coarse-grained realisations, effectively adding a new dimension to all such analyses. As alluded to, one can estimate the number of structural features at each scale ($A_t(\lambda)$ as multiples of $A_0(\lambda)$), and it will be interesting to correlate this number to other quantifiers of cortical structure, such as neuron numbers (Mota and Herculano-

Houzel, 2014), number of functional areas (Molnár et al., 2014) or the number of cortical columns (Kaas, 2012), possibly over different stages of development. More qualitatively, comparative neuroanatomical methods (Croxson et al., 2017; Mars et al., 2014) may be directly used to identify and contrast structures in coarse-grained cortices of more highly gyrified species with their analogues in less-gyrified species. One could then perhaps specify when evolution conserves and when it invents old and new cortical structures.

Given how broadly it has been verified, we expect the observed universality in cortical self-similar scaling to be robust to the details of the coarse-graining method. It would be very informative to test this proposition. For example, an alternative method inspired by (Yu et al., 2021) could be implemented, eschewing voxelization and dealing only with the flow of nested surfaces with self- and mutual- avoidance explicitly implemented. Going in the opposite direction, more detailed models for the mechanisms of cortical folding (see e.g. (Raznahan et al., 2011)) can be regarded as a type of reverse melting, and could perhaps be implemented and tested in a similar fashion as fine-graining procedures.

Empirically, the main result of this paper is the demonstration of universal self-similar scaling (Eqn. 3) for primate, and presumably mammalian, cortices. This was a proof-by-construction of fractality, a step beyond the usual box-counting approach. With this understanding, the previously observed scaling law (Eqn. 1) across species (Mota and Herculano-Houzel, 2015) and individuals (Wang et al., 2016) follows as consequence: all cortices are a different realisations of the same archetypal fractal shape, and thus collectively must obey the same scaling law. Note that the opposite did not have to be true: the scaling law across cortices does not necessarily imply scale-invariance within each cortex, nor the existence of an archetypal fractal brain shape. Thus, (3) is both a more strict test for any model for gyrification than (1), and may also represent an illuminating probe into the detailed mechanical stresses that must be its immediate cause, along with the underlying developmental mechanisms from which the latter arise. Ultimately, it hints at the possibility of deriving cortical scaling from some variational principle.

The most important implication from our results is that there is a *single mechanism*, conserved by evolution, that dictates cortical gyrification, with only a few morphological degrees of freedom:

the morphological complexity $S(\lambda)$ and the isometric size $I(\lambda)$. The scaling itself does not imply or favor any particular proposed mechanism (ours (Mota and Herculano-Houzel, 2015) included), and in fact all results in this paper are agnostic about this choice. Indeed, our previously proposed model (Mota and Herculano-Houzel, 2015) for cortical gyrification is very simple, which is both a strength and a weakness. There are many complex phenomena in nature that display simple and universal scaling that can be derived from first principles (Barenblatt, 1996; Gagler et al., 2022; West et al., 1997). In addition, recent results suggest simplicity and symmetry are generically favoured on statistical-ensemble grounds by evolution (Johnston et al., 2022). Our model correctly predicts the scaling law (Eqn. 1), but a more complete explanation for cortical gyrification is probably far more complex (Quezada et al., 2020) than can be accounted by such a simple model. Nevertheless, it provides an interpretation for the parameter K , which we have now shown to be highly conserved (in healthy adult individuals) across species, individuals, cortical regions, and spatial scales. In our previous model (Mota and Herculano-Houzel, 2015), K is a free parameter that captures the elasto-mechanical properties of neurons, axons, and cortical tissue in general. Thus, its invariance is likely a consequence of evolutionarily conserved elasto-mechanical properties of brain tissue. Conversely, changes in $K(\lambda)$, either during development, over aging or as a consequence of disease, may in the future be connected directly to specific changes in these mechanical properties. It is certainly rewarding that our results about the cortex’s large-scale morphology could inform our understanding of its micro-mechanics; but at the moment we can only speculate as to whether the latter’s conserved nature is a result of historical contingency, or was a selected for feature leading to some form of adaptive optimization.

More broadly, the interaction between brain development and evolution may also benefit from a scale-specific understanding. This may be important in elucidating what in cortical morphology is selected for by evolution, what is determined by physics; what is specified by genes, and what is emergent. Generally, the larger the cortical feature (i.e. from gyri to functional areas to lobes to hemispheres), the earlier during development it appears (Garcia et al., 2018; Zilles et al., 2013), and more broadly it is conserved over kinship (Pizzagalli et al., 2020) and phylogeny (Heuer et al., 2019; Valk et al., 2020). Coarse-graining to different scales will thus allow for retaining

only the common features between a specified degree of kinship and/or stage of development. Our work here was limited to summary statistics of entire cortical hemispheres, but future work will explore the extension of these methods to lobes and cortical areas, similarly to (Leiberg et al., 2021; Wang et al., 2019). This may help us precisely characterize the morphological differences between phylae and perhaps pinpoint the stage and location of morphological changes leading to congenital and neurodegenerative conditions. Ultimately, we hope this new framework for expressing and analyzing cortical morphology, besides revealing a hitherto hidden regularity of nature, can become a powerful tool to characterize and compare cortices of different species and individuals, across development and aging, and across health and disease.

Acknowledgements

We thank members of the Computational Neurology, Neuroscience & Psychiatry Lab (www.cnp-lab.com) for discussions on the analysis and manuscript; P.N.T. and Y.W. are both supported by UKRI Future Leaders Fellowships (MR/T04294X/1, MR/V026569/1). We thank Dirk Jan Ardesch and Martijn van den Heuvel for helpful discussions and NHP brain surface data.

References

- Dirk Jan Ardesch, Lianne H Scholtens, Siemon C de Lange, Lea Roumazeilles, Alexandre A Khrapitchev, Todd M Preuss, James K Rilling, Rogier B Mars, and Martijn P van den Heuvel. Scaling Principles of White Matter Connectivity in the Human and Nonhuman Primate Brain. *Cerebral Cortex*, 32(13):2831–2842, July 2022. ISSN 1047-3211. doi: 10.1093/cercor/bhab384.
- G.I. Barenblatt. *Scaling, Self-similarity, and Intermediate Asymptotics: Dimensional Analysis and Intermediate Asymptotics*. Cambridge Texts in Applied Mathematics. Cambridge University Press, 1996. ISBN 9780521435222. URL <https://books.google.com.br/books?id=r-Az53e-MTYC>.
- Katherine L. Bryant, Dirk Jan Ardesch, Lea Roumazeilles, Lianne H. Scholtens, Alexandre A. Khrapitchev, Benjamin C. Tandler, Wenchuan Wu, Karla L. Miller, Jerome Sallet, Martijn P. van den Heuvel, and Rogier B. Mars. Diffusion MRI data, sulcal anatomy, and tractography for eight species from the Primate Brain Bank. *Brain Structure and Function*, 226(8):2497–2509, November 2021. ISSN 1863-2661. doi: 10.1007/s00429-021-02268-x.
- Paula L Croxson, Stephanie J Forkel, Leonardo Cerliani, and Michel Thiebaut de Schotten. Structural Variability Across the Primate Brain: A Cross-Species Comparison. *Cerebral Cortex*, 28(11):3829–3841, 10 2017. ISSN 1047-3211. doi: 10.1093/cercor/bhx244. URL <https://doi.org/10.1093/cercor/bhx244>.
- Antonio Di Ieva. *The Fractal Geometry of the Brain*. Springer Series in Computational Neuroscience. Springer, 2016. ISBN 978-1-4939-3995-4. doi: 10.1007/978-1-4939-3995-4.
- G. N. Elston and Brendan Zietsch. Fractal analysis as a tool for studying specialization in neuronal structure: the study of the evolution of the primate cerebral cortex and human intellect. *Adv. Complex Syst.*, 8(2-3):217–227, 2005. URL <http://dblp.uni-trier.de/db/journals/advcs/advcs8.html#ElstonZ05>.
- David C. Van Essen. A tension-based theory of morphogenesis and compact wiring in the central

nervous system. *Nature*, 385(6614):313–318, January 1997. doi: 10.1038/385313a0. URL <http://www.nature.com/nature/journal/v385/n6614/abs/385313a0.html>.

Cassot Francis, Lauwers Frederic, Lorthois Sylvie, Puwanarajah Prasanna, and Duvernoy Henri. Scaling laws for branching vessels of human cerebral cortex. *Microcirculation*, 16(4):331–344, 2009. doi: 10.1080/10739680802662607.

S. L. Free, S. M. Sisodiya, M. J. Cook, D. R. Fish, and S. D. Shorvon. Three-Dimensional Fractal Analysis of the White Matter Surface from Magnetic Resonance Images of the Human Brain. *Cerebral Cortex*, 6(6):830–836, 11 1996. ISSN 1047-3211. doi: 10.1093/cercor/6.6.830. URL <https://doi.org/10.1093/cercor/6.6.830>.

Dylan C. Gagler, Bradley Karas, Christopher P. Kempes, John Malloy, Veronica Mierzejewski, Aaron D. Goldman, Hyunju Kim, and Sara I. Walker. Scaling laws in enzyme function reveal a new kind of biochemical universality. *Proceedings of the National Academy of Sciences*, 119(9): e2106655119, March 2022. doi: 10.1073/pnas.2106655119. URL <https://www.pnas.org/doi/10.1073/pnas.2106655119>. Publisher: Proceedings of the National Academy of Sciences.

Kara E. Garcia, Emma C. Robinson, Dimitrios Alexopoulos, Donna L. Dierker, Matthew F. Glasser, Timothy S. Coalson, Cynthia M. Ortinau, Daniel Rueckert, Larry A. Taber, David C. Van Essen, Cynthia E. Rogers, Christopher D. Smyser, and Philip V. Bayly. Dynamic patterns of cortical expansion during folding of the preterm human brain. *Proceedings of the National Academy of Sciences*, 115(12):3156–3161, 2018. doi: 10.1073/pnas.1715451115. URL <https://www.pnas.org/doi/abs/10.1073/pnas.1715451115>.

Katja Heuer, Omer Faruk Gulban, Pierre-Louis Bazin, Anastasia Osoianu, Romain Valabregue, Mathieu Santin, Marc Herbin, and Roberto Toro. Evolution of neocortical folding: A phylogenetic comparative analysis of mri from 34 primate species. *Cortex*, 118:275–291, 2019. ISSN 0010-9452. doi: <https://doi.org/10.1016/j.cortex.2019.04.011>. URL <https://www.sciencedirect.com/science/article/pii/S0010945219301704>. The Evolution of the Mind and the Brain.

Clara Ionescu, Alain Oustaloup, François Levron, Pierre Melchior, Jocelyn Sabatier, and Robin

De Keyser. A model of the lungs based on fractal geometrical and structural properties. *IFAC Proceedings Volumes*, 42(10):994–999, 2009. ISSN 1474-6670. doi: <https://doi.org/10.3182/20090706-3-FR-2004.00165>. URL <https://www.sciencedirect.com/science/article/pii/S1474667016387791>. 15th IFAC Symposium on System Identification.

Chi-Wen Jao, Chi Ieong Lau, Li-Ming Lien, Yuh-Feng Tsai, Kuang-En Chu, Chen-Yu Hsiao, Jiann-Horng Yeh, and Yu-Te Wu. Using fractal dimension analysis with the desikan–killiany atlas to assess the effects of normal aging on subregional cortex alterations in adulthood. *Brain Sciences*, 11(1), 2021. ISSN 2076-3425. doi: [10.3390/brainsci11010107](https://doi.org/10.3390/brainsci11010107). URL <https://www.mdpi.com/2076-3425/11/1/107>.

Kaide Jin, Tianqi Zhang, Marnie Shaw, Perminder Sachdev, and Nicolas Cherbuin. Relationship Between Sulcal Characteristics and Brain Aging. *Frontiers in Aging Neuroscience*, 10:339, November 2018. ISSN 1663-4365. doi: [10.3389/fnagi.2018.00339](https://doi.org/10.3389/fnagi.2018.00339). URL <https://www.ncbi.nlm.nih.gov/pmc/articles/PMC6240579/>.

Iain G. Johnston, Kamaludin Dingle, Sam F. Greenbury, Chico Q. Camargo, Jonathan P. K. Doye, Sebastian E. Ahnert, and Ard A. Louis. Symmetry and simplicity spontaneously emerge from the algorithmic nature of evolution. *Proceedings of the National Academy of Sciences*, 119(11): e2113883119, 2022. doi: [10.1073/pnas.2113883119](https://doi.org/10.1073/pnas.2113883119). URL <https://www.pnas.org/doi/abs/10.1073/pnas.2113883119>.

Jon H. Kaas. Evolution of columns, modules, and domains in the neocortex of primates. *Proceedings of the National Academy of Sciences*, 109(supplement_1):10655–10660, 2012. doi: [10.1073/pnas.1201892109](https://doi.org/10.1073/pnas.1201892109). URL <https://www.pnas.org/doi/abs/10.1073/pnas.1201892109>.

Jan Karbowski. Scaling of brain metabolism and blood flow in relation to capillary and neural scaling. *PLoS ONE*, 6(10), 2011. doi: [10.1371/journal.pone.0026709](https://doi.org/10.1371/journal.pone.0026709).

Valerij G. Kiselev, Klaus R. Hahn, and Dorothee P. Auer. Is the brain cortex a fractal? *NeuroImage*, 20(3):1765–1774, 2003. ISSN 1053-8119. doi: <https://doi.org/10.1006/nimg.2003.2670>.

1016/S1053-8119(03)00380-X. URL <https://www.sciencedirect.com/science/article/pii/S105381190300380X>.

Włodzimierz Klonowski. *Fractal Analysis of Electroencephalographic Time Series (EEG Signals)*, pages 413–429. Springer, 08 2016. ISBN 978-1-4939-3993-0. doi: 10.1007/978-1-4939-3995-4_25.

Evgeniy Lebed, Claudia Jacova, Lei Wang, and Mirza Faisal Beg. Novel surface-smoothing based local gyrification index. *IEEE Trans. Medical Imaging*, 32(4):660–669, 2013. URL <http://dblp.uni-trier.de/db/journals/tmi/tmi32.html#LebedJWB13>.

Karoline Leiberger, Christoforos Papasavvas, and Yujiang Wang. Local morphological measures confirm that folding within small partitions of the human cortex follows universal scaling law. In Marleen de Bruijne, Philippe C. Cattin, Stéphane Cotin, Nicolas Padoy, Stefanie Speidel, Yefeng Zheng, and Caroline Essert, editors, *Medical Image Computing and Computer Assisted Intervention – MICCAI 2021*, pages 691–700, Cham, 2021. Springer International Publishing. ISBN 978-3-030-87234-2.

Cirong Liu, Frank Q. Ye, Cecil Chern-Chyi Yen, John D. Newman, Daniel Glen, David A. Leopold, and Afonso C. Silva. A digital 3D atlas of the marmoset brain based on multi-modal MRI. *NeuroImage*, 169:106–116, 2018. doi: 10.1016/j.neuroimage.2017.12.004.

Cirong Liu, Frank Q. Ye, John D. Newman, Diego Szczupak, Xiaoguang Tian, Cecil Chern-Chyi Yen, Piotr Majka, Daniel Glen, Marcello G. P. Rosa, David A. Leopold, and Afonso C. Silva. A resource for the detailed 3d mapping of white matter pathways in the marmoset brain. *Nature Neuroscience*, 23(2):271–280, 2020. doi: 10.1038/s41593-019-0575-0.

Cristina Llinares-Benadero and Víctor Borrell. Deconstructing cortical folding: Genetic, cellular and mechanical determinants. *Nature Reviews Neuroscience*, 20(3):161–176, 2019. doi: 10.1038/s41583-018-0112-2.

Gabriele Angelo Losa. *Fractals in Biology and Medicine*. John Wiley & Sons, Ltd, 2011. ISBN 9783527600908. doi: <https://doi.org/10.1002/3527600906.mcb.201100002>. URL <https://onlinelibrary.wiley.com/doi/abs/10.1002/3527600906.mcb.201100002>.

- Christopher R. Madan. Creating 3D visualizations of MRI data: A brief guide. *F1000Research*, 4: 466, 2015. doi: 10.12688/f1000research.6838.1.
- Christopher R Madan. Improved understanding of brain morphology through 3d printing: A brief guide. *Research Ideas and Outcomes*, 2:e10398, 2016. doi: 10.3897/rio.2.e10398.
- Christopher R. Madan. Robust estimation of sulcal morphology. *Brain Informatics*, 6(1):5, June 2019. ISSN 2198-4026. doi: 10.1186/s40708-019-0098-1. URL <https://doi.org/10.1186/s40708-019-0098-1>.
- Christopher R. Madan and Elizabeth A. Kensinger. Cortical complexity as a measure of age-related brain atrophy. *NeuroImage*, 134(Supplement C):617–629, July 2016. ISSN 1053-8119. doi: 10.1016/j.neuroimage.2016.04.029. URL <http://www.sciencedirect.com/science/article/pii/S1053811916300519>.
- B. B. Mandelbrot. *The fractal geometry of nature*. W. H. Freeman and Comp., New York, 3 edition, 1983.
- Benoit Mandelbrot. How long is the coast of britain? statistical self-similarity and fractional dimension. *Science*, 156(3775):636–638, 1967. doi: 10.1126/science.156.3775.636. URL <https://www.science.org/doi/abs/10.1126/science.156.3775.636>.
- Rogier B. Mars, Franz-Xaver Neubert, Lennart Verhagen, Jerome Sallet, Karla L. Miller, Robin I. Dunbar, and Robert A. Barton. Primate comparative neuroscience using magnetic resonance imaging: Promises and challenges. *Frontiers in Neuroscience*, 8, 2014. doi: 10.3389/fnins.2014.00298.
- C. Marzi, M. Giannelli, C. Tessa, M. Mascalchi, and S. Diciotti. Toward a more reliable characterization of fractal properties of the cerebral cortex of healthy subjects during the lifespan. *Sci Rep*, 10(16957), 2020. doi: 10.1038/s41598-020-73961-w. URL <https://www.nature.com/articles/s41598-020-73961-w#content>.

- Chiara Marzi, Marco Giannelli, Carlo Tessa, Mario Mascalchi, and Stefano Diciotti. Fractal analysis of mri data at 7 t: How much complex is the cerebral cortex? *IEEE Access*, 9:69226–69234, 2021. doi: 10.1109/ACCESS.2021.3077370.
- Zoltán Molnár, Jon H. Kaas, Juan A. de Carlos, Robert F. Hevner, Ed Lein, and Pavel Němec. Evolution and development of the mammalian cerebral cortex. *Brain, Behavior and Evolution*, 83(2):126–139, 2014. doi: 10.1159/000357753.
- Bruno Mota and Suzana Herculano-Houzel. All brains are made of this: A fundamental building block of brain matter with matching neuronal and glial masses. *Frontiers in Neuroanatomy*, 8, 2014. doi: 10.3389/fnana.2014.00127.
- Bruno Mota and Suzana Herculano-Houzel. Cortical folding scales universally with surface area and thickness, not number of neurons. *Science* 349(6243):74–77, 2015. doi: 10.1126/science.aaa9101. URL <https://doi.org/10.1126/science.aaa9101>.
- Bruno Mota, Sandra E. Dos Santos, Lissa Ventura-Antunes, Débora Jardim-Messeder, Kleber Neves, Rodrigo S. Kazu, Stephen Noctor, Kelly Lambert, Mads F. Bertelsen, Paul R. Manger, Chet C. Sherwood, Jon H. Kaas, and Suzana Herculano-Houzel. White matter volume and white/gray matter ratio in mammalian species as a consequence of the universal scaling of cortical folding. *Proceedings of the National Academy of Sciences*, 116(30):15253–15261, 2019. doi: 10.1073/pnas.1716956116. URL <https://www.pnas.org/doi/abs/10.1073/pnas.1716956116>.
- Kate Noonan, Stanley Colcombe, Russell Tobe, Maarten Mennes, Melissa Benedict, Alexis Moreno, Laura Panek, Shaquanna Brown, Stephen Zavitz, Qingyang Li, Sharad Sikka, David Gutman, Saroja Bangaru, Rochelle Tziona Schlachter, Stephanie Kamiel, Ayesha Anwar, Caitlin Hinz, Michelle Kaplan, Anna Rachlin, Samantha Adelsberg, Brian Cheung, Ranjit Khanuja, Chaogan Yan, Cameron Craddock, Vincent Calhoun, William Courtney, Margaret King, Dylan Wood, Christine Cox, Clare Kelly, Adriana DiMartino, Eva Petkova, Philip Reiss, Nancy Duan, Dawn Thompsen, Bharat Biswal, Barbara Coffey, Matthew Hoptman, Daniel Javitt, Nunzio Pomara, John Sidtis, Harold Koplewicz, Francisco Castellanos, Bennett Leventhal, and Michael Milham. The nki-rockland sample: A model for accelerating the pace of discovery science in psychiatry.

Frontiers in Neuroscience, 6, 2012. ISSN 1662-453X. doi: 10.3389/fnins.2012.00152. URL <https://www.frontiersin.org/article/10.3389/fnins.2012.00152>.

Fabrizio Pizzagalli, Guillaume Auzias, Qifan Yang, Samuel R. Mathias, Joshua Faskowitz, Joshua Boyd, Armand Amini, Denis Rivière, Katie L. McMahon, Greig I. de Zubicaray, Nicholas G. Martin, Jean-François Mangin, David C. Glahn, John Blangero, Margaret J. Wright, Paul M. Thompson, Peter Kochunov, and Neda Jahanshad. The reliability and heritability of cortical folds and their genetic correlations across hemispheres. *Communications Biology*, 2020. doi: 10.1038/s42003-020-01163-1. URL <https://doi.org/10.1038/s42003-020-01163-1>.

Michael J. Plank and Simon Benhamou. Random walk models in biology. *Journal of the Royal Society, Interface*, 5(35):21, August 2008. ISSN 2198-4026. doi: 10.1098/rsif.2008.0014. URL <https://doi.org/10.1098/rsif.2008.0014>.

Sebastian Quezada, Yohan van de Looij, Nadia Hale, Shreya Rana, Stéphane V Sizonenko, Courtney Gilchrist, Margie Castillo-Melendez, Mary Tolcos, and David W Walker. Genetic and microstructural differences in the cortical plate of gyri and sulci during gyrification in fetal sheep. *Cerebral Cortex*, 30(12):6169–6190, 07 2020. ISSN 1047-3211. doi: 10.1093/cercor/bhaa171. URL <https://doi.org/10.1093/cercor/bhaa171>.

Hamed Rabiei, Frédéric Richard, Olivier Coulon, and Julien Lefèvre. Local spectral analysis of the cerebral cortex: New gyrification indices. *IEEE Transactions on Medical Imaging*, 36(3): 838–848, 2017. doi: 10.1109/TMI.2016.2633393.

Armin Raznahan, Phillip Shaw, Francois Lalonde, Mike Stockman, Gregory L. Wallace, Dede Greenstein, Liv Clasen, Nitin Gogtay, and Jay N. Giedd. How Does Your Cortex Grow? *The Journal of Neuroscience*, 31(19):7174–7177, May 2011. ISSN 0270-6474. doi: 10.1523/JNEUROSCI.0054-11.2011. URL <https://www.ncbi.nlm.nih.gov/pmc/articles/PMC3157294/>.

Natalie Reznikov, Matthew Bilton, Leonardo Lari, Molly M. Stevens, and Roland Kröger. Fractal-like hierarchical organization of bone begins at the nanoscale. *Science*, 360(6388):eaao2189, 2018.

doi: 10.1126/science.aao2189. URL <https://www.science.org/doi/abs/10.1126/science.aao2189>.

Lisa Ronan and Paul C. Fletcher. From genes to folds: A review of cortical gyrification theory. *Brain Structure and Function*, 220(5):2475–2483, 2014. doi: 10.1007/s00429-014-0961-z.

M. Schaer, M. B. Cuadra, L. Tamarit, F. Lazeyras, S. Eliez, and J. P. Thiran. A Surface-Based Approach to Quantify Local Cortical Gyrification. *IEEE Transactions on Medical Imaging*, 27(2):161–170, February 2008. ISSN 0278-0062. doi: 10.1109/TMI.2007.903576.

Meredith A Shafto, Lorraine K Tyler, Marie Dixon, Jason R Taylor, James B Rowe, Rhodri Cusack, Andrew J Calder, William D Marslen-Wilson, John Duncan, Tim Dalgleish, et al. The cambridge centre for ageing and neuroscience (cam-can) study protocol: a cross-sectional, lifespan, multidisciplinary examination of healthy cognitive ageing. *BMC neurology*, 14(1):204, 2014.

Tuomas Tallinen, Jun Young Chung, John S. Biggins, and L. Mahadevan. Gyrification from constrained cortical expansion. *Proceedings of the National Academy of Sciences*, 111(35):12667–12672, 2014. doi: 10.1073/pnas.1406015111. URL <https://www.pnas.org/doi/abs/10.1073/pnas.1406015111>.

Jason R Taylor, Nitin Williams, Rhodri Cusack, Tibor Auer, Meredith A Shafto, Marie Dixon, Lorraine K Tyler, Richard N Henson, et al. The cambridge centre for ageing and neuroscience (cam-can) data repository: structural and functional mri, meg, and cognitive data from a cross-sectional adult lifespan sample. *Neuroimage*, 144:262–269, 2017.

Sofie L. Valk, Ting Xu, Daniel S. Margulies, Shahrzad Kharabian Masouleh, Casey Paquola, Alexandros Goulas, Peter Kochunov, Jonathan Smallwood, B. T. Thomas Yeo, Boris C. Bernhardt, and Simon B. Eickhoff. Shaping brain structure: Genetic and phylogenetic axes of macroscale organization of cortical thickness. *Science Advances*, 6(39):eabb3417, September 2020. ISSN 2375-2548. doi: 10.1126/sciadv.abb3417. URL <https://advances.sciencemag>.

org/content/6/39/eabb3417. Publisher: American Association for the Advancement of Science
Section: Research Article.

Yujiang Wang, Joe Necus, Marcus Kaiser, and Bruno Mota. Universality in human cortical folding in health and disease. *PNAS*, 2016. doi: 10.1073/pnas.1610175113. URL <https://doi.org/10.1073/pnas.1610175113>.

Yujiang Wang, Joe Necus, Luis Peraza Rodriguez, Peter Neal Taylor, and Bruno Mota. Human cortical folding across regions within individual brains follows universal scaling law. *Communications Biology*, 2(1):1–8, May 2019. ISSN 2399-3642. doi: 10.1038/s42003-019-0421-7. URL <https://www.nature.com/articles/s42003-019-0421-7>.

Yujiang Wang, Karoline Leiberg, Tobias Ludwig, Bethany Little, Joe H Necus, Gavin Winston, Sjoerd B Vos, Jane de Tisi, John S Duncan, Peter N Taylor, and Bruno Mota. Independent components of human brain morphology. *NeuroImage*, 226:117546, February 2021. ISSN 1053-8119. doi: 10.1016/j.neuroimage.2020.117546. URL <https://www.sciencedirect.com/science/article/pii/S1053811920310314>.

Geoffrey B. West, James H. Brown, and Brian J. Enquist. A General Model for the Origin of Allometric Scaling Laws in Biology. *Science*, 276(5309):122, March 1997. doi: <https://doi.org/10.1126/science.276.5309.122>. URL <https://www.science.org/doi/10.1126/science.276.5309.122>.

Chris Yu, Caleb Brakensiek, Henrik Schumacher, and Keenan Crane. Repulsive surfaces. *ACM Trans. Graph.*, 40(6), dec 2021. ISSN 0730-0301. doi: 10.1145/3478513.3480521. URL <https://doi.org/10.1145/3478513.3480521>.

Kechen Zhang and Terrence J. Sejnowski. A universal scaling law between gray matter and white matter of cerebral cortex. *Proceedings of the National Academy of Sciences*, 97(10):5621–5626, 2000. doi: 10.1073/pnas.090504197. URL <https://www.pnas.org/doi/abs/10.1073/pnas.090504197>.

Karl Zilles, Nicola Palomero-Gallagher, and Katrin Amunts. Development of cortical folding during evolution and ontogeny. *Trends in Neurosciences*, 36(5):275–284, 2013. ISSN 0166-2236. doi: <https://doi.org/10.1016/j.tins.2013.01.006>. URL <https://www.sciencedirect.com/science/article/pii/S0166223613000180>.

Supplementary

S1 Primate species and cortical surface reconstruction

S1.1 Human data

To study healthy human adults, we used the Human Connectome Project (HCP) MRI data, available at <https://db.humanconnectome.org/> (?), obtained using a Siemens Skyra scanner with 0.7mm isotropic voxel size. We used the HCP minimally pre-processed Freesurfer data output, which provided the pial and white matter surface meshes we required. We selected five random subjects in the age category 22-25 y.o. and show one example subject (103414) in the main text, and the remaining subjects in Suppl. S2.

To study the alterations associated with human ageing, we used T1 and T2 weighted MRI brain scans from The Cambridge Centre for Ageing and Neuroscience (Cam-CAN) dataset (available at <http://www.mrc-cbu.cam.ac.uk/datasets/camcan/> (Shafto et al., 2014; Taylor et al., 2017)). Cam-CAN used a 3T Siemens TIM Trio System with 1 mm isotropic voxel size (for more details see (Shafto et al., 2014; Taylor et al., 2017)). From the Cam-CAN dataset we retained 644 subjects that successfully completed preprocessing (with Freesurfer recon-all) without errors. From these subjects we randomly selected 5 females and 5 males between the ages of 19-21 (forming the 20 y.o. cohort); we also randomly selected 5 females and 5 males between the ages of 79-81 (forming the 80 y.o. cohort).

To confirm the ageing results, we also obtained an independent dataset from the Nathan Kline Institute (NKI)/Rockland sample (Nooner et al., 2012) (http://fcon_1000.projects.nitrc.org/indi/pro/nki.html) using the same procedure as described for the CamCAN dataset.

The MR images of both CamCAN and NKI datasets were first preprocessed by the FreeSurfer 6.0 pipeline *recon-all*, which extracts the grey-white matter boundary as well as the pial surface. These boundaries were then quality checked and manually corrected where needed.

For all three datasets, we obtained the pial and white matter surfaces for further analysis. In the current work, the analysis is always hemisphere based, as in our previous work (Mota and

Herculano-Houzel, 2015; Wang et al., 2016). We did not perform a more regionalised analysis, which is also possible (Wang et al., 2019). Future work using the principle demonstrated here can be directly extended to derive regionalised measures across scales.

S1.2 Non-human primate data

Rhesus Macaque MRI scans were carried out at the Newcastle University Comparative Biology Centre. Macaques were trained to be scanned while awake and sat in a primate chair. Both T1 weighted MP-RAGE and T2 weighted RARE sequences were acquired, using a vertical MRI scanner (Biospec 4.7 Tesla, Bruker Biospin, Ettlingen, Germany).

Scans were processed using a custom macaque MRI pipeline, incorporating ANTs, SPM, FreeSurfer and FSL. Briefly, this involved the creation of precursor mask in SPM, denoising (ANTs DenoiseImage) and debiasing (ANTs N4BiasFieldCorrection, and Human Connectome BiasField-Correction script), creation of a final mask in SPM and then processing in FreeSurfer (using a modified version of the standard FreeSurfer processing pipeline). Reconstructed pial and white matter surfaces were visually quality controlled in conjunction with the MR images.

The marmoset MRI structural scan was collected as part of the development of the NIH marmoset brain atlas (Liu et al., 2018, 2020). Data was collected ex vivo from a 4.5-year-old male marmoset using a T2-star weighted 3D FLASH sequence using a horizontal MRI scanner (Biospec 7 Tesla, Bruker Biospin, Ettlingen, Germany).

A total of ten scans were collected and averaged into one final image. In combination with scans from other modalities, cortical boundaries were manually delineated on each coronal slice. Boundaries were then refined through comparisons with other atlases. Volumetric data was then converted to surfaces using a custom pipeline involving an intermediate generation of high-resolution mesh data (Madan, 2015), decimation (Madan, 2016), and remeshing. Reconstructed pial and white matter surfaces were visually quality controlled in conjunction with the MR images.

The remaining NHP MRI and subsequent brain surface extraction is detailed in (Ardesch et al., 2022; Bryant et al., 2021), and provided to the authors in a readily processed format. Briefly, a range of specialised scanners were used to acquire optimal images for each species. FreeSurfer 6.0

with some modifications was used for surface reconstruction, complemented by FSL, ANTS, and Matlab. All surfaces were visually inspected for accuracy and consistency across datasets.

S1.3 Comparative neuroanatomy data

The comparative neuroanatomy dataset for different mammalian species is the same as previously published (Mota and Herculano-Houzel, 2015). Note that for this dataset, we only had numerical values for the total and exposed surface area, as well as average cortical thickness estimates. We did not perform any analysis across scales in this dataset (hence surfaces were not required), but only used it as a reference dataset.

S2 Scaling properties by species

S2.1 Obtaining the scaling law

From the coarse-grain procedure (Fig. 1), we obtain surface meshes for the pial and white matter surface at each spatial scale. From those, we derive exposed area, total pial surface area, and average cortical thickness as described in Methods. However, the coarse-graining procedure, by itself, barely changes the exposed surface area, and only changes the total surface area minimally (Fig. ?? A). As the voxel size changes at each scale, it only starts to affect the exposed area at very large scales, where effectively the voxels are no longer a good description of the shape of the skull. Thus, if we scatter the raw datapoints from the coarse-graining procedure in the plane of the scaling law, there is barely any variance in the data (Fig. ?? B). Even after zooming in, we see an almost vertical line (Fig. ?? B). This is expected and is not evidence for or against our hypothesis.

Instead, we need to transform the data into a perspective that makes sense to be seen in the scaling law plane. Instead of thinking of the coarse-graining procedure as a process that re-renders the cortex at increasing voxel sizes, we can instead think of the procedure as rescaling the original cortical mesh into increasingly smaller sizes, and re-rendering it with the same fixed voxel size. The analogy using Britain's coastline is that instead of measuring the coastline with increasingly

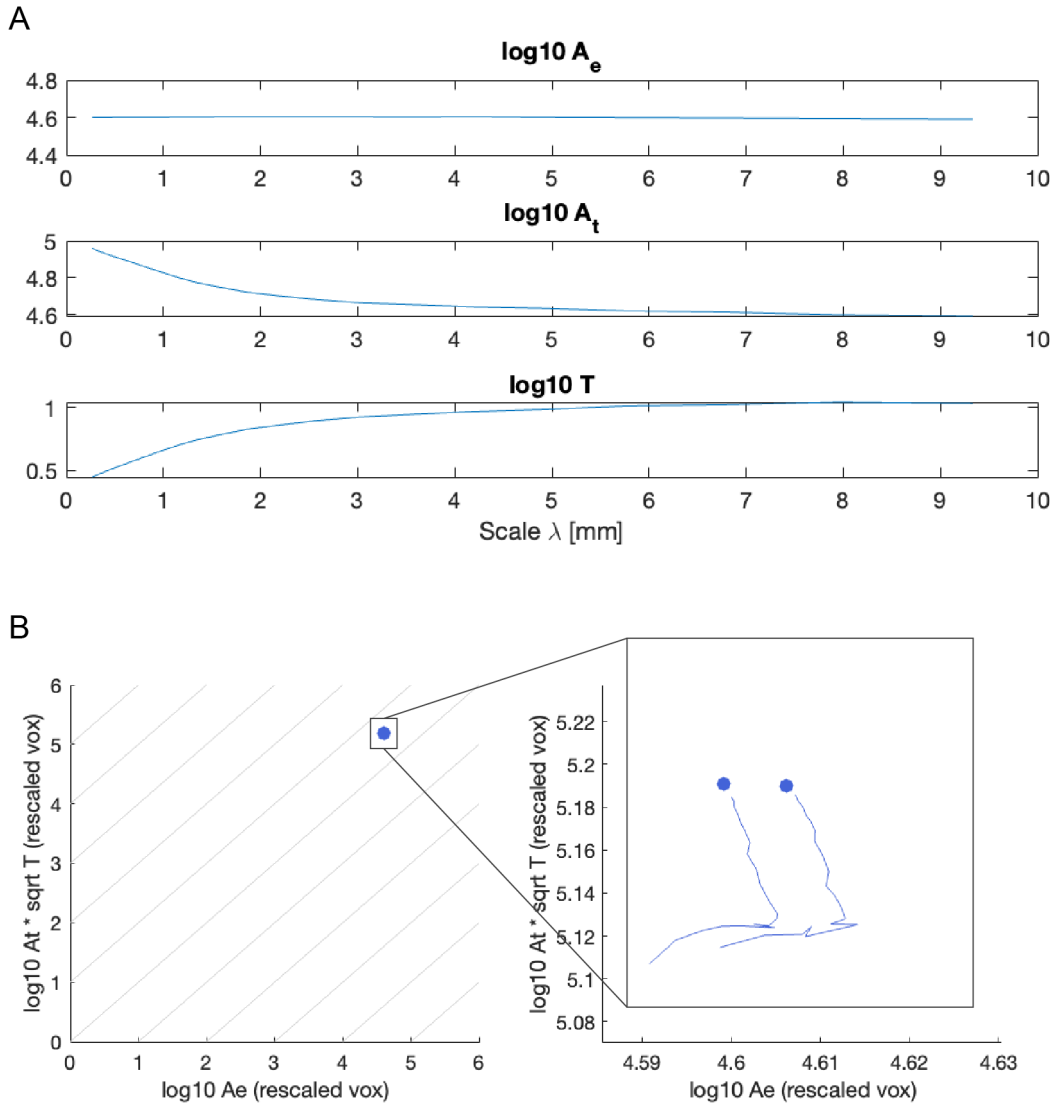


Figure S2.1: Unscaled quantities cannot be used to verify scaling law. A: The exposed surface area A_e barely changes across scales, and A_t only changes minimally. **B:** Plotted in the scaling law plane (as Fig. 2) the datapoints barely have any variance, and overlap each other substantially. Even after zooming in, the trace for the the coarse-graining procedure (solid line) is virtually a vertical line (with a small artifactual ‘tail’ coming from very large voxel sizes).

smaller rulers, we resize the map of the coastline to increasingly smaller sizes, but keep the size of the ruler the same. Both procedures are equivalent and produce the same fractal dimension.

To achieve this procedure, we re-scaled our measurements of A_e , T and A_t by the voxel size

(λ) and a fixed factor (l_r) :

$$\begin{aligned} A_e^r &= \frac{A_e}{(\lambda \times l_r)^2} \\ A_t^r &= \frac{A_t}{(\lambda \times l_r)^2} \\ T^r &= \frac{T}{(\lambda \times l_r)}. \end{aligned} \tag{4}$$

As we used isometric cubes as voxels, the voxel size refers to the length of a single side. E.g. $\lambda = 1$ if we used a isometric $1 \times 1 \times 1mm^3$ voxel.

l_r is a fixed factor for each cortical hemisphere, and does not change with λ . We use it to systematically shift all the datapoints within a range, such that the re-scaled quantities are not larger than those from the original cortical meshes. One can easily verify that l_r will not change the slope or offset of any scaling law, but simply represents a constant shift to all datapoints. In our data, some of the re-scaled quantities would indeed be larger than those from the original cortical meshes, as the voxel size we choose are limited at the smaller end only by computational resources. I.e. we can use very small voxel sizes (relative to the mesh), which after re-sizing would yield very large values of A_e^r , A_t^r , and T^r . To avoid this, we chose l_r simply as the ratio of the I (isometric term) of the mesh at the smallest scale we used relative to the original mesh, divided by the λ of the smallest scale:

$$l_r = \frac{1}{\lambda_s} \times \frac{I_s}{I_o}, \tag{5}$$

where λ_s is the smallest voxel size used for a particular cortex, I_s is the corresponding I for this cortex at the smallest voxel size.

Finally, I_o is the I term for the original cortical mesh. Indeed, the ratio of $\frac{I_s}{I_o}$ is always close to, but larger than one in our dataset. Thus, we can see in Fig. 2 A that most traces start very close to the original datapoint, indicating that our finest scale is reconstructing the original surfaces well.

Note that the re-scaling is isometric, meaning that it only affects I , but does not change the data in the $K \times S$ plane (Fig. 3). Rescaling by a factor proportional to λ^2 can therefore be

understood as distributing the datapoints along the I axis, while l_r can be understood as fixing the position in the I axis relative to the I of the original mesh.

Fig. 2 A is produced with these rescaled quantities as described above. The only final step in producing Fig. 2 A, and in calculating the associated slopes, is the removal of artifactual datapoints where $\frac{A_t}{A_e} < 0$, which can occur at very large voxel sizes relative to the cortical mesh.

The algorithmic implementation in MATLAB can be found on Github: TO BE ADDED!

S2.2 Details for each species

In the following, we will show the detailed data for each species in terms of their scaling behaviour in Fig. S2.2.

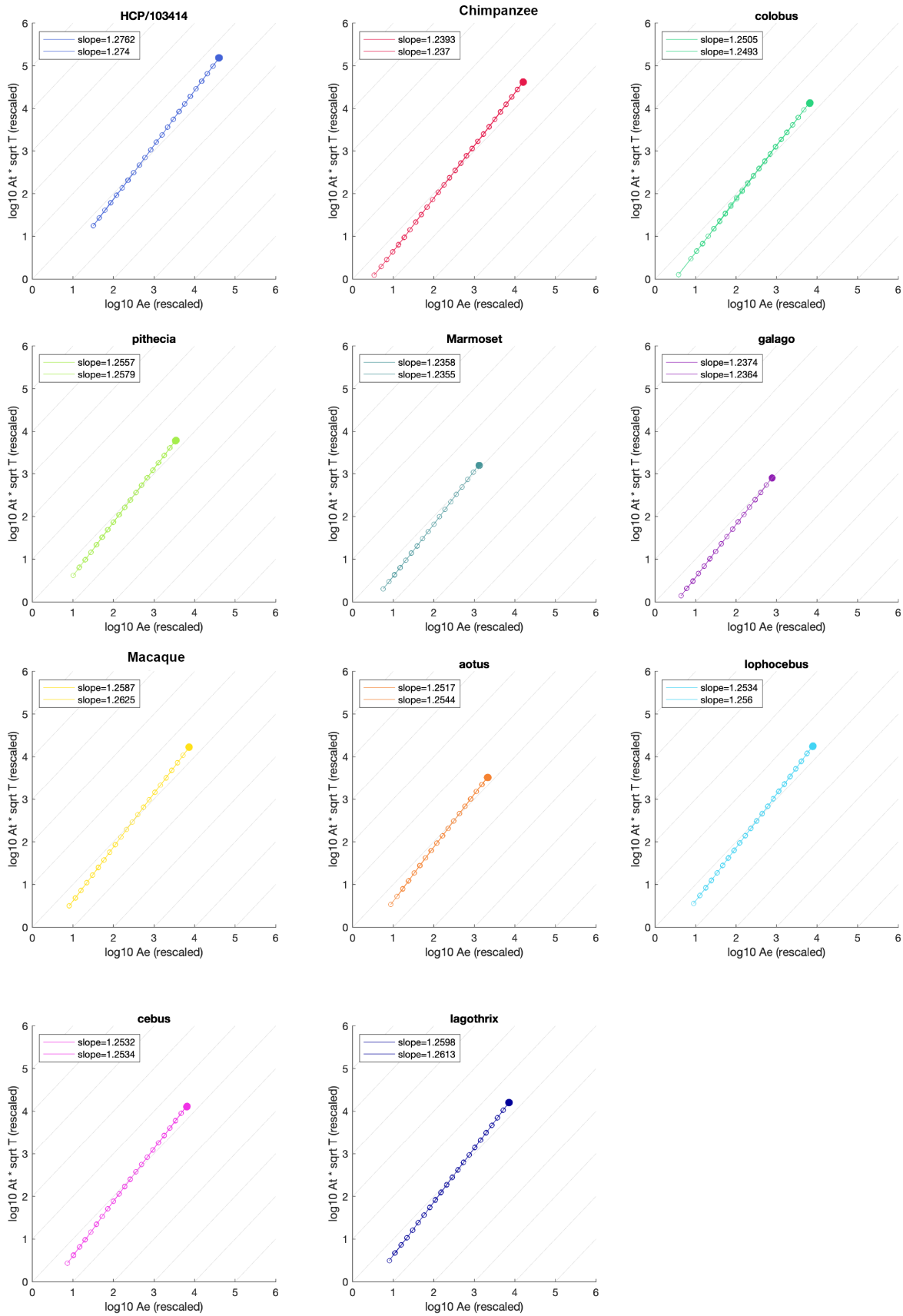


Figure S2.2: Detailed scaling plots for each species. Filled circle is the original mesh, empty circle are datapoints from the coarse-graining algorithm. Empty circles are connected by a line for visualisation. Two hemispheres are analysed separated for each species, although datapoints overlap substantially in plot. Slope estimates are given at top left corner in each plot.

S3 Validation with non-brain shapes: walnuts

We chose to apply our coarse-graining procedure to a shape that may appear similar to a brain, but is not a mammalian brain. The walnut has been likened to the shape of the brain before, and it was therefore a obvious choice. We obtained an MRI-reconstructed surface for two walnut halves <http://www.brainmapping.org/MCpers/nuts.html>. Only one surface was available for each half (equivalent to the pial surface). Hence we isometrically down-scaled the surface to obtain a reasonable inner surface (equivalent to the white matter surface). Note these surfaces were used as a negative control of a non-brain shape, and not necessarily as an accurate representation of walnuts.

Fig. S3.1 shows the scaling behaviour of the walnut relative to some of our primate brains. We observed a scaling behaviour, but with a distinctly lower slopes (walnut 1: $\alpha = 1.191$, $CI = [1.185 \ 1.196]$; walnut 2: $\alpha = 1.193$, $CI = [1.187 \ 1.198]$) than the primate brains. The offset is also visibly distinct, although this is not to be over-interpreted, as the “cortical thickness” of the walnut was somewhat arbitrarily chosen.

Fig. S3.2 shows the $K \times S$ projection of the walnut relative to some of our primate brains. The walnuts appear very distinct compared to the primate brains, as their K is changing with S and their S is is distinctively lower.

Both figures together support our statement that the walnut shape, although showing some likeness to brains, is a distinct shape. It does not obeying the universal scaling law and has a distinct fractal dimension. This also further supports the validity of our coarse-graining algorithm, and the scaling law is not a by-product of our methods.

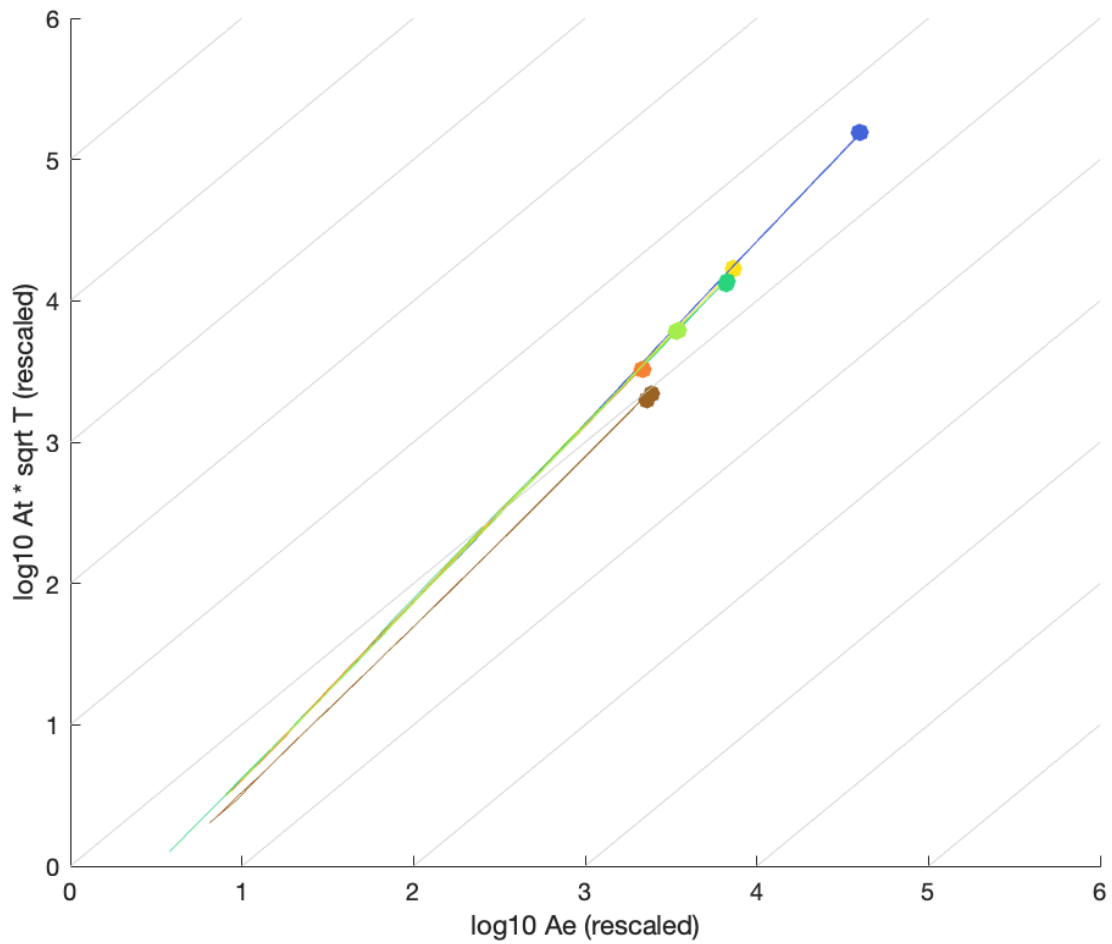


Figure S3.1: Scaling behaviour of the walnut relative to primate brains. All colour coding and plotting convention as Fig. 2. Only a subset of primate brains is shown for clarity. The two walnuts are shown as brown data points and traces.

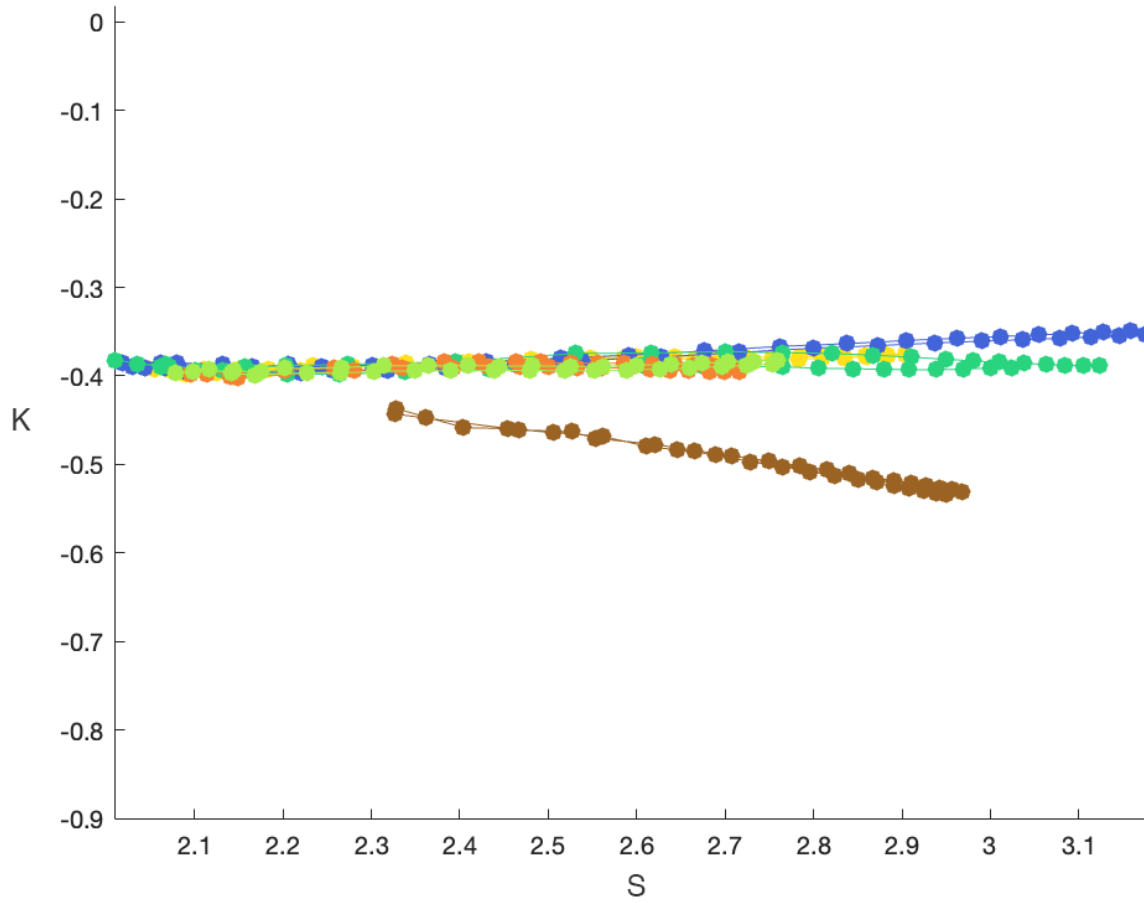


Figure S3.2: $K \times S$ plane plot for the walnut relative to primate brains. The two walnuts are shown as brown data points and traces. All other colour coding as in Fig. 3. Only a subset of primate brains is shown for clarity. Individual datapoints underlying the trace for each species/walnut are shown to demonstrate sufficient sampling.

S4 Ageing process, all morphometric variables

For completeness, here we also show all the morphometric variables across scales in the 20 y.o. and 80 y.o. cohort in Fig. S4.1, and the corresponding effect sizes in Fig. S4.2. As expected, A_e shows very little difference between the two cohorts. I , S , and T show some effects at scales smaller than 4 mm, but the effect decreases monotonously for higher scales.

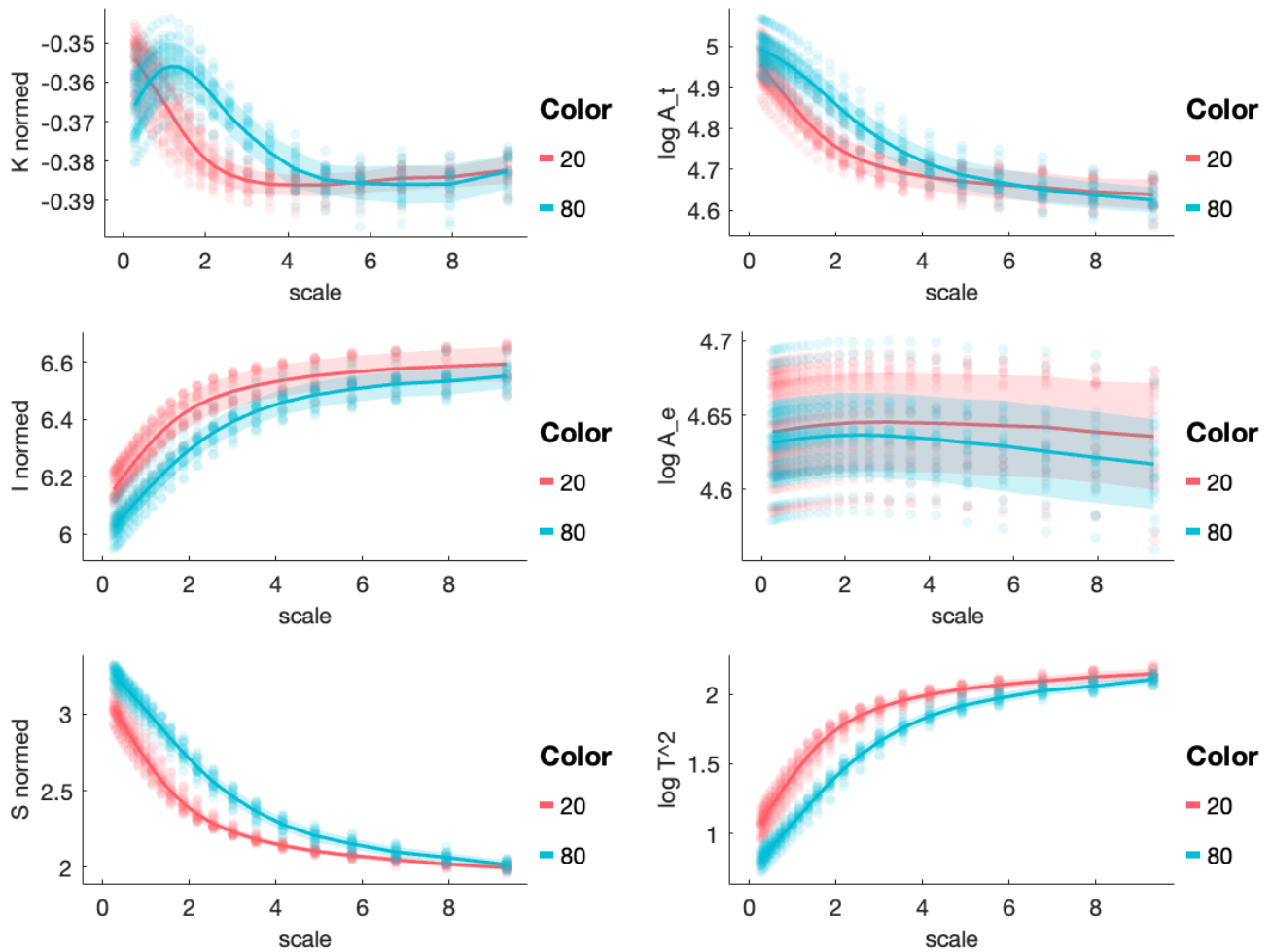


Figure S4.1: All morphological variables across scales in the 20 y.o. and 80 y.o. cohort.

Effect sizes Age 20 vs age 80 (CamCAN)

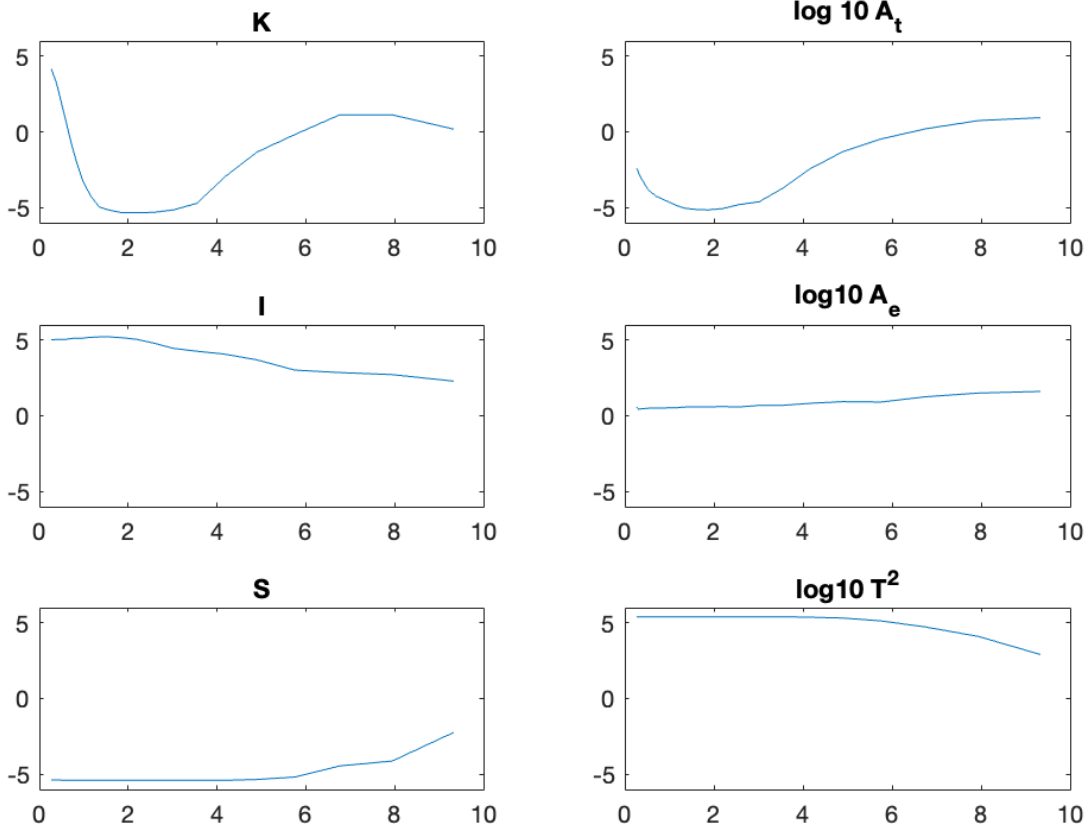


Figure S4.2: Effect size between the 20 y.o. and 80 y.o. cohort in all morphological variables. Effect size is measured as the ranksum z statistic between the two groups.

S5 Ageing process, confirmed in independent dataset

To confirm that our observed ageing effect was not driven by sample or data-specific properties, we also analysed an independent dataset (NKI) with the same methods (see Section S1). Here, we show the equivalent figures to Fig. S4.1 and Fig. S4.2 for the NKI data in Fig. S5.1 and Fig. S5.2. The same qualitative patterns can be seen in all plots, including the scale-specific effects in K and A_e at around 2 mm.

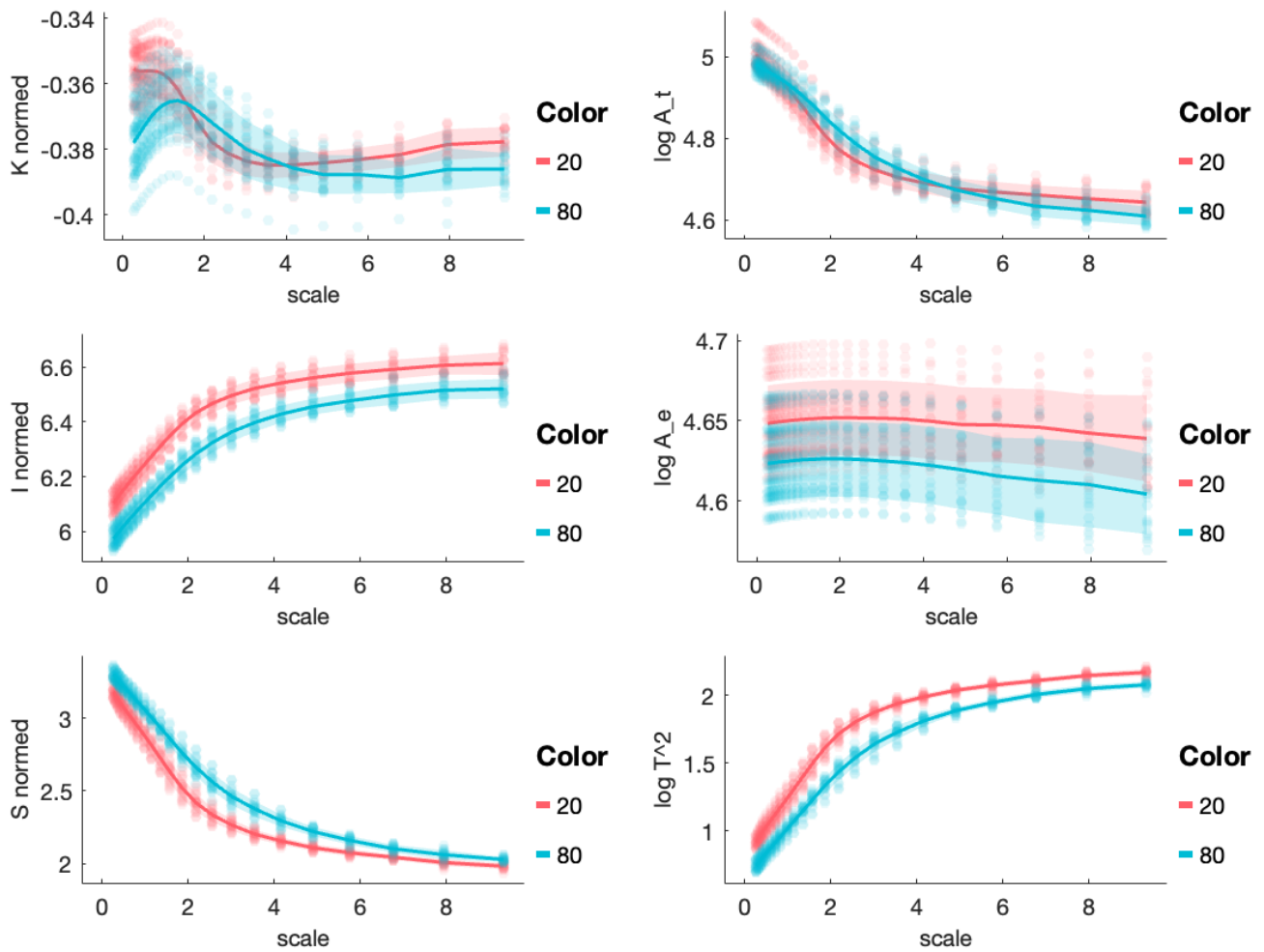


Figure S5.1: All morphological variables across scales in the 20 y.o. and 80 y.o. cohort in a separate (NKI) dataset.

Effect sizes Age 20 vs age 80 (NKI)

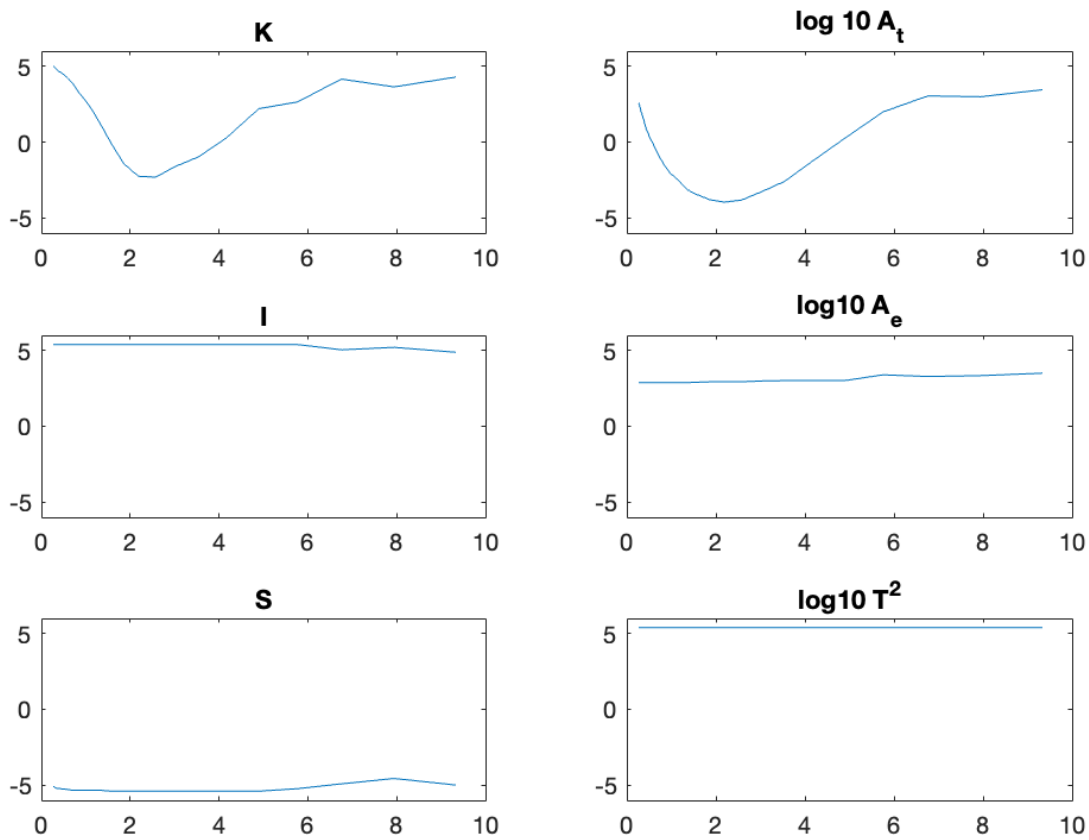


Figure S5.2: Effect size between the 20 y.o. and 80 y.o. cohort in all morphological variables in a separate (NKI) dataset. Effect size is measured as the ranksum z statistic between the two groups.

S6 Morphometric relations and the range of validity of the fractal approximation

There are many geometrical quantities that describe aspects of entire cortical hemispheres. But most information contained in such summary morphometric measures is captured, exactly or to good approximations, by the three used in Eqn (1): The pial (or total) surface area A_t , exposed surface area A_e , and average cortical thickness T . Other quantities, like the gyrification index $g = \frac{A_t}{A_e}$, or the Grey Matter and Total volumes, can be expressed as products of power laws of these quantities; and the logarithm of products of power laws are linear combinations of the logarithms of the constituting variables, with their exponents as coefficients. Thus, the morphology of a given cortex can be fairly summarized as point in a 3-dimensional morphometric space with components given by $\log A_t$, $\log A_e$ and $\log T^2$ (the last exponent guarantees all axes have the same dimension of $\log[Area]$).

This logarithmic structure guarantees that the quantities denoted by products of power laws of the original variables correspond to vectors in the morphometric space: The increase and decrease of their values occur along these vectors, and the planes perpendicular to each vector denote all configurations with the same value for the associated variable. For example, $G = \log g = \log A_t - \log A_e$, the vector in the morphometric space associated with the gyrification ratio, defines a vector with coefficients $\{1, -1, 0\}$.

The quantities K , S and I used in Sec. 3.2 likewise define vectors in morphometric space, which are all orthogonal to one another. These can be normalized, so that the sum of their squared coefficients equals unity. In this case, expressing cortical shape in the morphometric space in terms of the original variables or the new variables amounts simply to a change in orthonormal base.

Figs. 2 and 3 can be then regarded as particular 2D snapshots, taken from a certain direction, of a 3D set of points.

Of particular note, those vectors with a sum of coefficients equal to zero correspond to dimensionless variables. Any such vector is perpendicular to the I direction, and lie on the $K \times S$

plane.

In this framework, we can picture the successive coarse-graining of a cortex, as described in Sec. 3.1, as a trajectory in this morphometric space. Empirically, Sec. 3.1, as codified by Eqn. 3, finds that the trajectories in morphometric space for all studied primates are linear, and largely overlap along a line of constant K . For cortical morphology, the first fact implies scale-invariance, the second implies universality.

Aging, development and the progression of neurodegenerative conditions likewise each correspond to different morphometric trajectories.

Now consider a morphometric trajectory, corresponding to the coarse-graining of a cortex up to the point of lysencephaly, i.e., to the spatial scale λ_{lys} such that $A_t(\lambda_{lys}) = A_e(\lambda_{lys})$. In the idealized case (but very close to empirical, as seen in Sec. 3.1), all points along the trajectory should follow Eqn (3), starting at the original values for the morphometric measures and ending at the intersection of the $K = constant$ coarse-graining line and the $g = 1$ line that defines the limit for lysencephaly (points with $g < 1$ are clearly not plausible). This trajectory correspond to a span for the values of each morphometric measure: For dimensionless morphometric measures, such span is full specified by Eqn (3). For all others, one needs also to specify the voxel rescaling. The scheme described in Sec. S2.1 simply guarantees that, for a constant $k = A_t A_e^{-\frac{5}{4}} T^{\frac{1}{2}}$, the fundamental area element $A_0 = \frac{T^2}{k^4} = \frac{A_e^5}{A_t^4}$ (and thus also the average thickness T) is kept constant for all realisations of the coarse-graining process. We can regard these as approximations of the same original cortex, all drawn with the same resolution, but in ever smaller isometric sizes.

This choice of spatial scale then allows our identification of A_0 as the typical size of the smallest morphological features and at the same time the limit area between lysencephaly and gyrencephaly.

This same choice also enable us to easily compute the span of the various morphometric measures over coarse-graining: Each will range between its original value (expressed as a function of the original values for A_t , A_e and T), and their value at spatial scale λ_{lys} , where $A_t(\lambda_{lys}) = A_e(\lambda_{lys}) = A_0$: We simply replace A_t and A_e by $A_0 = \frac{A_e^5}{A_t^4}$, and T by $\sqrt{A_0 k^4}$. The ratios between the initial and final values of all morphometric measures are given as powers of g , imbuing the

gyrification index with a new significance.

We list below the spans for all such morphometric measures ($S = \log s$, $K = \log k$ and $I = \log v_I$)

Morphometric measure	Original Value =	Span \times	Value at lissencephalic limit
T^2	T^2	1	$A_0 k^4$
A_e	A_e	g^4	A_0
A_t	A_t	g^5	A_0
V_{total}	$\approx \frac{2}{9\sqrt{3}\pi} A_e^{\frac{3}{2}}$	g^6	$\approx \frac{2}{9\sqrt{3}\pi} A_0^{\frac{3}{2}}$
V_{GM}	$A_t T$	g^5	$A_0^{\frac{3}{2}} k^2$
g	$\frac{A_t}{A_e}$	g	1
$N_{structures}$	$\frac{A_t^5}{A_e^5}$	g^5	1
k	$A_t A_e^{-\frac{5}{4}} T^{\frac{1}{2}}$	1	k
s	$A_t^{\frac{3}{2}} A_e^{\frac{3}{4}} T^{-\frac{9}{2}}$	$g^{\frac{21}{2}}$	k^{-9}
v_I	$A_t A_e T^2$	g^9	$A_0^3 k^4$
\hat{k}	$A_t^{\frac{4}{\sqrt{42}}} A_e^{-\frac{5}{\sqrt{42}}} T^{\frac{2}{\sqrt{42}}}$	1	\hat{k}
\hat{s}	$A_t^{\frac{2}{\sqrt{14}}} A_e^{\frac{1}{\sqrt{14}}} T^{-\frac{6}{\sqrt{14}}}$	$g^{\frac{18}{\sqrt{14}}}$	$\hat{k}^{-3\sqrt{3}}$
\hat{v}_I	$A_t^{\frac{1}{\sqrt{3}}} A_e^{\frac{1}{\sqrt{3}}} T^{\frac{2}{\sqrt{3}}}$	$g^{3\sqrt{3}}$	$A_0 \hat{k}^{\sqrt{14}}$